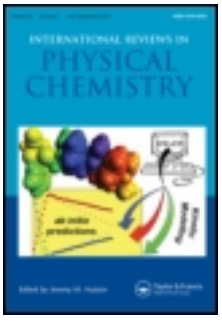

International Reviews in Physical Chemistry

Publication details, including instructions for authors and subscription information:
http://www.tandfonline.com/loi/trpc20

Spontaneous electric fields in solid films: spontelectrics

D. Field [a b], O. Plekan [a c], A. Cassidy [a], R. Balog [a], N.C. Jones [b] & J. Dunger [a]

[a] Department of Physics and Astronomy, Aarhus University, Ny Munkegade Building 1520, DK 8000, Aarhus C, Denmark

[b] ISA, Department of Physics and Astronomy, Aarhus University, Ny Munkegade Building 1520, DK 8000, Aarhus C, Denmark

[c] Sincrotrone Trieste, S.C.p.A. di Interesse Nazionale, 34149 Basovizza, Trieste, Italy

Published online: 12 Mar 2013.

To cite this article: D. Field, O. Plekan, A. Cassidy, R. Balog, N.C. Jones & J. Dunger (2013) Spontaneous electric fields in solid films: spontelectrics, International Reviews in Physical Chemistry, 32:3, 345-392, DOI: 10.1080/0144235X.2013.767109

To link to this article: http://dx.doi.org/10.1080/0144235X.2013.767109

International Reviews in Physical Chemistry, 2013
Vol. 32, No. 3, 345–392, http://dx.doi.org/10.1080/0144235X.2013.767109

Spontaneous electric fields in solid films: spontelectrics†

D. Field[a,b]*, O. Plekan[a,c], A. Cassidy[a], R. Balog[a], N.C. Jones[b] and J. Dunger[a]

[a]*Department of Physics and Astronomy, Aarhus University, Ny Munkegade Building 1520, DK 8000, Aarhus C, Denmark;* [b]*ISA, Department of Physics and Astronomy, Aarhus University, Ny Munkegade Building 1520, DK 8000, Aarhus C, Denmark;* [c]*Sincrotrone Trieste, S.C.p.A. di Interesse Nazionale, 34149 Basovizza, Trieste, Italy*

(*Received 19 December 2012; final version received 14 January 2013*)

When dipolar gases are condensed at sufficiently low temperature onto a solid surface, they form films that may spontaneously exhibit electric fields in excess of 10^8 V/m. This effect, called the 'spontelectric effect', was recently revealed using an instrument designed to measure scattering and capture of low energy electrons by molecular films. In this review it is described how this discovery was made and the properties of materials that display the spontelectric effect, so-called 'spontelectrics', are set out. A discussion is included of properties that differentiate spontelectrics from ferroelectrics and other species in which spontaneous polarisation may be found.

Spontelectric films may be composed of a number of quite mundane dipolar molecules that involve such diverse dipolar species as propane, nitrous oxide or methyl formate. Experimental results are presented for spontelectrics illustrating that the spontelectric field generally decreases monotonically with increasing deposition temperature, with the exception of methyl formate that shows an increase beyond a critical range of deposition temperature. Films of spontelectric material show a Curie temperature above which the spontelectric effect disappears. Heterolayers may also be laid down creating potential wells on the nanoscale.

A model is put forward based upon competition between dipole alignment and thermal disorder, which is successful in reproducing the variation of the degree of dipole alignment and the spontelectric field with deposition temperature, including the behaviour of methyl formate. This model and associated data lead to the conclusion that the spontelectric effect is new in solid-state physics and that spontelectrics represent a new class of materials.

Keywords: ferroelectrics; dipole orientation; Curie points; heterostructures; polarised solids; spontelectrics

*Corresponding author. Email: dfield@phys.au.dk

†Dedicated to the memory of Jean-Pierre Ziesel, highly valued both as a wonderful scientist and a great friend.

Contents PAGE

1. Introduction

1.1. *The discovery of spontaneously polarised materials, 'spontelectrics', and their salient properties*

Four years ago or thereabouts, we initiated at Aarhus a programme of research designed to study the interaction of very low-energy electrons with solid material. This followed many

years of experience in controlling electron beams down to energies of a few meV, with an energy resolution in the beam of $\leqslant 1$ meV, for the study of electron scattering in gases [1–3]. These studies had thrown up a number of fundamental phenomena in electron–molecule interactions such as virtual state scattering [4], the coupling between elastic and dissociative channels [5] and phase shifts and time delays in low energy scattering [6]. We sought to find if these and other phenomena had counterparts in electron scattering in solids. There was almost no data in the literature concerning the scattering and attachment of very low-energy electrons involving solid material and the field was wide open for new discoveries. What we faced instead was the discovery of a new class of spontaneously polarised solids. This deflected us from the study of electron scattering by solids to the nature of the solids themselves, in which the low-energy electron beam became a probe of the properties of the solids. These solids have been dubbed 'spontelectric' and they form the subject of the current review.

What was found was as follows. Electrons, formed by synchrotron photoionisation [2,3] of argon at a well-defined potential, were allowed to impinge on solid material in the form of a film prepared by low temperature deposition from the gas phase. Give or take some small potential differences, a current should pass into the sample when the sample is held at a potential more positive than that at which the electrons were formed, assuming that there is an energy band in the solid which they may enter. Under this condition, electrons may then pass through the solid undergoing scattering. Alternatively, electrons may be trapped within the solid in gap states and an induced current may be measured. The latter was the case for water ice at 40 K where small repulsive potentials of typically ~ -10 mV on the ice were observed to build up during electron irradiation [7]. However, similar films, but formed of nitrous oxide (N_2O), were found to *attract* electrons rather than repel them. A negative bias had to be applied to the metallic substrate on which the N_2O film was formed in order to null the current [8]. The bias increased linearly with film thickness and could be of many volts. The inference was that the N_2O surface was spontaneously biased electrically positive. This unexpected property was rapidly confirmed by a series of experiments described in Ref. [8], the original paper in which the effect was described. The conclusion was drawn there, substantially strengthened by subsequent work, that the spontelectric effect arises through intrinsic alignment of the permanent dipoles of the constituent species.

Succeeding studies [9–12] have revealed that an extensive class of solids composed of polar molecules are spontelectric and one may presently hazard the assertion that gas-phase deposition of dipolar species generally yields spontelectric films and exceptionally does not. Species identified differ radically in chemical structure, spanning a variety of molecules from propane to methyl formate and dihydrofuran. Their common property is that these molecules possess permanent gas-phase dipoles. By some means, as yet unknown in any detail, polar molecules deposited from the gas phase assume a dipole aligned structure in the solid film. This gives rise to net macroscopic polarisation whose presence is felt through a surface potential on the film. Only two species tested in the temperature range down to 38 K were found not to show the spontelectric effect, namely water ice which is discussed below in Section 1.2 and carbonyl sulphide (OCS). Why it is that the latter species, which has a gas-phase dipole moment of 0.715 D, does not show the spontelectric effect remains presently unknown. It may perhaps form crystalline films [13] with a structure determined by other forces than dipole–dipole, a property that is very likely to preclude the spontelectric effect, as we describe in subsequent sections.

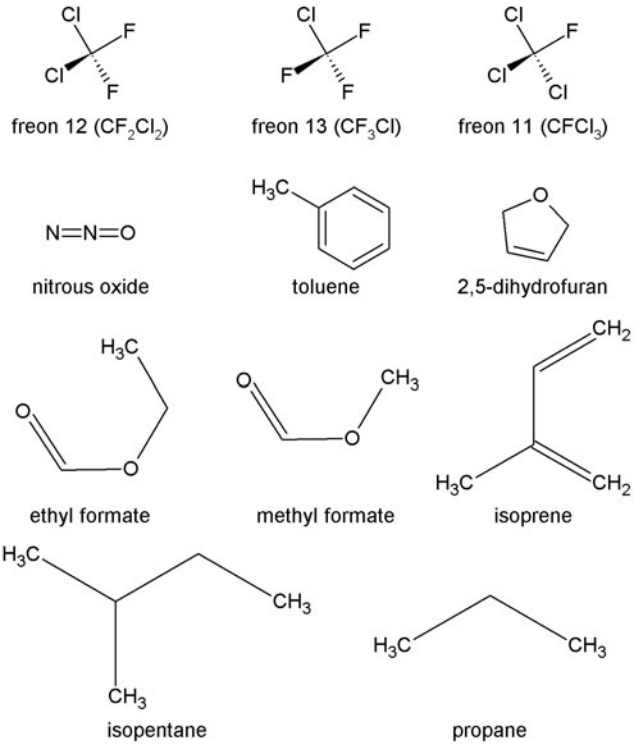

Figure 1. Spontelectric materials so far identified, with their chemical structures.

The spontelectric materials so far identified are shown in Figure 1. This list of molecules could doubtless be made to grow rapidly. At present, the emphasis is upon learning the properties of spontelectric materials more than extending the list.

The salient observed properties of spontelectrics may be summarised as follows:

- On forming a film by gas-phase deposition under ultra-high vacuum of a spontelectric material, a potential, typically of several volts, appears spontaneously on the surface of the film.
- This potential may be either positive or negative and gives rise to a corresponding spontelectric field in the film.
- The potential is linearly proportional to the thickness of the film. The highest voltage measured was 38 V on a $\sim$1100 monolayer film of N_2O.
- The spontelectric field depends on the temperature at which the film is deposited. It is in general less for higher temperatures.
- For one material (methyl formate), the spontelectric field at first falls but then *increases* with temperature beyond a critical temperature of deposition.
- At greater than a certain temperature of deposition, no spontelectric effect can be observed.

- Warming of a spontelectric film in general causes at first little change in the spontaneous potential on the surface of the film. A critical temperature is reached at which the spontelectric effect decays abruptly. By analogy with ferromagnetism, this is referred to as the Curie point.
- Subsequent cooling to below the Curie point has not been observed to reintroduce a surface potential.
- The spontelectric potential is in general stable with time, at least over a period of hours.
- The nature of the surface upon which spontelectric films are deposited has essentially no bearing on the values of surface potential.
- Spontelectric films can be laid down one on the other and behave approximately independently, making feasible the creation of any desired structure of electric fields on the nanoscale.

1.2. *Do spontelectric materials represent a new phenomenon in solid-state physics?*

The question that forms the title of this section itself spawns several others. First, has the spontelectric phenomenon ever been recorded before the 'discovery' publication in Ref. [8]? Second, if this phenomenon has not been clearly described in other work, how could such a fundamental property of thin films have been missed (or ignored) after so many years of solid-state science? Third, do not ferroelectric materials also show spontaneous polarisation and may not spontelectrics be a subgroup of ferroelectrics?

On an historical note, Smyth and Hitchcock [14] performed measurements of molecular rotation in solid ammonia and hydrogen sulphide through measurements of the dielectric constant at 5 kHz from ~80 K and up. They found no evidence for rotation in solid ammonia but observed an abrupt and reversible change (with a hint of hysteresis) in the dielectric constant at ~100 K of solid H_2S. The authors note that this is suggestive of a transition to an ordered state. In view of the present results, the onset of hindered rotation may have been associated with dipole ordering in the bulk (although the authors do not suggest this). However, they report the reversibility of the phenomenon on cooling. This is not observed for spontelectrics, as noted in Sections 1.1 and 3.

Instead of retreating 80 years [14], we move forward to the work of Kutzner performed 40 years ago [15]; here, we find that a variety of molecules, including CO, N_2O and H_2O, formed ices which were stated to show spontaneous polarisation. These investigations claim to have established the presence of potentials on the surface of films of material. Kutzner reported the measurement of the displacement current flowing as layers of material were deposited and attributed this current to the presence of surface charge and thus polarisation in the material. This work therefore suggests the existence of a spontelectric phenomenon and constitutes a broad hint that spontaneous dipole alignment may take place in films of dipolar species. We note, however, with reference to H_2O ice films, that our own work, using the technique described in detail in Section 2 below, shows that there is no permanent dipole alignment in such films [7], in contradiction to the work of Kutzner [15]. Results in Ref. [7] are consistent with the standard view that the bulk structure of water ice laid down at low pressure and temperature is dictated by hydrogen bonding (see for example Ref. [16] which also discusses limited polar ordering in ice). This brings into question both the interpretation

of the work of Kutzner and more recent work [17,18], using the Kelvin probe technique, which concluded that water ice is, as the latter reference puts it, ferroelectric in character. The sceptical view presented here with regard to the spontaneous polarisation of water ice is echoed by standard textbooks on ice structure [19].

1.2.1. *Surface dipoles*

Remaining on the tack of 'has the spontelectric phenomenon ever been seen before?', the adsorption of a monolayer of polar molecules on surfaces is well-known to give rise to a surface dipole [20,21]. Dipolar image effects and displacement of charge between the substrate and the adsorbate, for example, from a metal to an organic film, give rise to surface potentials, of either sign, which are typically of a few hundred meV. However, the adsorption of further layers does not change the apparent work function markedly, that is, there is no additional change in the surface potential after several layers are added. This very well-documented phenomenon, see for example Ref. [22], is therefore associated with the surface–adsorbate interface and is not a bulk property of the film. Thus the observation here that the surface potential increases linearly with increasing film thickness, maintaining an inherent polarisation, which gives rise to an apparently constant electric field in the film, sets the phenomena associated with spontelectric films apart from surface dipole potentials.

1.2.2. *Solid organic films*

Spontaneous surface potentials and accompanying electrostatic fields are well-known to occur in solid organic films [23–29]. These, therefore, display properties more closely resembling those of spontelectrics than do the properties of the surface dipole layer. In the following sections, we first very briefly mention some relevant properties of organic films in general, taking polyimide films as representative of these films. We then review the properties of the organic semiconductor tris (8-quinolinolato) aluminium (Alq_3) in a little more detail. This material is singled out since films of Alq_3, apparently uniquely, have properties that at least superficially resemble those of spontelectrics. Ferroelectric properties of organic films [30] are compared with spontelectrics in Section 1.2.4.

Polyimide films [31] yield a surface potential that increases with the number of layers of material. This increase continues progressively more weakly until a polyimide film thickness of typically 30–50 monolayers (ML) is achieved. The increase in surface potential then ceases for thicker films. Values of the surface potential vary according to the nature of the substrate. Values of the potential *increase* with substrate temperature and can achieve $\sim$1 V. Uniquely, in the case of thin films of Alq_3 [32–34], the potential on the film surface increases linearly with thickness and may achieve values of 28 V. The corresponding electric field in the film is $\sim 10^7$ V/m. Values of surface potential vary strongly according to the nature of the substrate, showing for example roughly half as large a surface potential when deposited on Al as upon Au (figure 3 of Ref. [33]) under otherwise the same conditions. The sign of the field, however, appears unaffected by the nature of the substrate [34]. Temporal decay of the electric field was observed on warming of the films. This has been reported to be due to electron injection from the metal substrate through a potential barrier,

for example, of 1.3 eV for Al [33], rather than through thermally induced reordering as in spontelectrics, as described in Sections 3 and 4. Films of Alq_3 are also strongly photosensitive [32], a typical surface potential decaying to zero on absorption of 5 mW/cm^2 for 20 s at 400 nm, a wavelength at which Alq_3 strongly absorbs [33]. All authors agree that the origin of the spontaneous surface potential in Alq_3 is net dipole alignment. The reported photosensitivity for Alq_3 is typical of such dipole aligned systems [35] and the model of dipole alignment as the origin of the surface potential is reinforced by reports of second harmonic generation by films of Alq_3 [32]. The origin of dipole alignment remains uncertain but to quote the most recent view [34] 'the molecular geometric effect originating from the molecular shape of Alq_3 is the origin of the non-centrosymmetric molecular alignment'. In this connection, chemical effects in which three ligands bind to the surface dictate the most favourable posture of Alq_3 on the surface. Reference to the properties of spontelectrics set out in 1.1 shows that spontelectrics behave quite differently from Alq_3 in a number of fundamental respects, such as behaviour with temperature or sensitivity to the surface on which material is laid down.

1.2.3. *How could such a fundamental property as the spontelectric effect of thin films have been missed?*

One may certainly wonder how the build-up of volts of potential on the surface of thin films has not been recorded after so many years of solid state science, *pace* the work of Kutzner [15]. A search of the literature reveals that X-ray photoelectron spectroscopy (XPS) of N_2O has shown evidence of small energy shifts in the apparent binding energy as a function of film thickness for layers up to 21 ML at 32 K. These shifts were attributed to charging effects of the films [36] but may have been due to the unsuspected spontelectric nature of the N_2O films. In general, however, XPS and other electron spectroscopies are carried out on very thin layers, typically a few ML or less, where spontelectric shifts would not be apparent. Moreover the dose of photoelectrons through the surface in (say) synchrotron radiation-based XPS is likely to be sufficient to destroy any spontaneous surface polarisation, which may arise due to the spontelectric nature of films, as we discuss in more detail below and in Section 3.5. Nevertheless, the spontelectric phenomenon could in principle be the origin of shifts and broadening of XPS peaks for thicker films.

Experiments where the spontelectric nature of films would be most likely to be detected would be those in which charging of films has been measured by direct illumination of cryofilms with electron beams – much as in our experiments described in Section 2. The pioneers in this field have been Sanche and co-workers: see Refs. [37–39] and numerous references therein. However, as we now show, the currents of electrons used in all previous experiments to our own, in which currents are typically $\sim$200 fA at maximum, overwhelm any spontaneous polarisation of the film that may be present and destroys the spontaneous surface potential. A specific example [40] makes this clear. The electric field in the film is related to the effective charge per unit area, that is the polarisation, at the surface of the film divided by the permittivity of the vacuum, ε_0 [32]. If we take the case of N_2O at 40 K, the electric field in the film has been inferred from experiment [9] to be 9.72×10^7 V/m and the polarisation charge on the surface of N_2O at 40 K is $\sim 1.7 \times 10^{-3}$ C/m^2. In Ref. [40] of Sanche and coworkers, a current of 0.12 nA of electrons was allowed to fall on a target (of solid CO_2 in that case) whose area defined a charge delivered per second of 10^{-3} C/m^2. Given an efficiency of

charge capture of 30% for N_2O [8], any surface potential would be removed, were the film composed of N_2O, in a few seconds of irradiation. Noting that currents in such experiments are generally ten or more times larger than in Ref. [40], it is evident why the spontelectric effect has not been observed previously by this otherwise direct method. In Section 3.5, we describe experiments on N_2O, which involve the reduction of the surface potential through irradiation with an electron beam, which corroborate the above statement.

1.2.4. *May not spontelectrics be a subgroup of ferroelectrics?*

Ferroelectric materials show spontaneous polarisation. The defining characteristic of ferroelectrics is switchable polarisation between two or more discrete states on application of an applied 'coercive' field and the related hysteresis under these applied fields [41]. Ferroelectric materials also display further properties such as piezoelectric, flexoelectric and electrostrictive effects [42] in which the polarisation of the material is coupled to its deformation. None of these phenomena, including switchable polarisation under a coercive field, has yet been investigated for spontelectrics, although they are likely to be encountered for these materials in some form. Ferroelectrics, moreover, continue to be a very active topic of research at the fundamental level, addressing such questions as the minimum size requirement for polarisation switching [43] or the identity of the driving force of permanent polarisation, the latter referring to the concept of electronic ferroelectricity rather than the conventional ionic displacement concept [44]. Both from an observational and a descriptive point of view, the spontelectric effect is very much in its infancy compared with the topic of ferroelectrics.

Notwithstanding, it is possible clearly to differentiate between organic ferroelectrics and spontelectrics. We concentrate here upon low mass organic ferroelectrics, such as the first organic ferroelectric, thiourea, since those classes of crystalline ferroelectrics which rely on ionic displacement to create a dipolar unit cell, or on proton transfer or hydrogen bonding to create aligned dipoles, are evidently fundamentally different from spontelectrics [30]. First, the similarities between spontelectrics and organic ferroelectrics: (i) ferroelectric organics show (or are presumed to show) a macroscopic spontaneous polarisation [41], *P*. This is measured through the hysteresis displayed under the influence of the coercive field, although to quote Ref. [41] '… the value of *P* is never measured directly as an equilibrium property', (ii) both organic ferroelectrics and spontelectrics in general show a Curie point, (iii) both rely upon polarisation created through the ordering of the dipoles in the film in order to create their special properties. Second, we list the differences: (i) the properties of spontelectric films may be reproduced by a model which does not require that the films are composed of domains (Section 4), whereas the presence of domains is a general property of ferroelectric materials [45] (but see for example Ref. [43]) and may be the determining factor in their ferroelectric properties [46] (ii) a cycle of thermal hysteresis [45,47–49], characteristic of ferroelectrics and generally readily observable, has not been experimentally detected in spontelectrics, (iii) the behaviour of polarisation with temperature of deposition observed for methyl formate (Section 3.2), with an increase in the spontelectric effect beyond a critical temperature, has not been observed for any ferroelectric material. This behaviour is shown to be a consequence of a general model for spontelectrics set out in Section 4. (iv) Spontelectric properties are intrinsically generated through dipole–dipole interactions, an aspect that again is reflected in the model for spontelectrics in Section 4. By contrast, ferroelectric properties are dictated, in comparable organic ferroelectrics, by interactions that are extrinsic to dipole–

dipole interactions. This makes for considerable difficulty and lack of success in identifying organic ferroelectric systems, an aspect that is discussed in some detail in Ref. [30]. The contrast with spontelectrics is striking since almost all small organics which we have tested show spontelectric behaviour (see Section 1.1).

We incline to the view that the answer to the title of this Section, 'Do spontelectric materials represent a new phenomenon in solid state physics?' is that spontelectrics are physically distinct from all other systems which show spontaneous macroscopic polarisation, namely certain polyimide films and ferroelectrics. Thus we propose that spontelectrics represent a new phenomenon in solid state physics.

Section 2 is devoted to technical details of the experimental method through which spontelectric behaviour was identified. Section 3 describes experimental data for a variety of molecules (see Figure 1), with special emphasis on N_2O, the group of species CF_3Cl, CF_2Cl_2, $CFCl_3$ and methyl formate. An example of a multilayer system for the creation of nanoscale potential structures is also included here. Section 4 sets out a theoretical model that describes the strength of the spontelectric effect as a function of the temperature of deposition of films of material.

2. The experimental technique for measuring spontelectric potentials

2.1. *The principle of measurement of surface potentials*

The potentials on film surfaces are measured using the principle that an electron beam formed at some point at a certain potential can just reach another point at the same potential, potential barriers apart. Thus, if electrons are formed at a known potential, the potential of their destination can be measured by the bias that must be applied either to their point of formation or their destination such that a current just begins to flow. The accuracy with which this bias can be measured depends on the energy resolution in the electron beam and the sensitivity of the detection system. The spontaneous potential appearing on the surface of spontelectric films is therefore measured by applying a bias potential to the system and effectively adjusting this bias in order to null the current. Since electrons are formed at nominally 0 V with an energy of $\sim$5 meV (see below), the beam should therefore just be able to reach a target when the target is itself at this same nominal zero (less 5 mV). If the surface of the target were not at zero but rather, say, at +5 V, due to a spontaneous formation of an electric field within the film, then in order to ensure that the electrons only just reach the target it would be necessary to bias the target, or the point of formation of the electrons, 5 V accordingly negative or positive. Measurement of the bias required to locate the onset of a measureable current, therefore, gives the potential on the surface of the film.

There is a small correction to be made to establish a true zero difference between the clean gold substrate and the potential of formation of the electrons. This arises from the difference between the work function of the gold substrate and the graphite-covered walls of the photoionisation chamber in which electrons are formed, as described below. This difference is measured for each series of experiments; a typical value of $\sim$0.25 V is found in agreement with standard figures.

A crucial difference between the present experiments and earlier work relating to electron irradiation of molecular films, save Ref. [7], is that here the dose of electrons [50] is two to three orders of magnitude lower (see also Section 1.2.3). Thus, we interrogate the material while perturbing it to a minimum, in particular by the avoidance of strong negative charging

or the concomitant removal of the surface potential in a spontelectric material. We give a quantitative demonstration of this point in Section 3.5.

2.2. *The electron source for measurement of surface potentials*

As indicated previously, the surface potential is measured by interrogating the surface with an electron beam. The electron beam has a maximum current typically of 200 fA. The essential elements of the apparatus are shown in Figure 2. Synchrotron radiation using the SGM2 beam line on the ASTRID storage ring at Aarhus University, where all experiments described here were performed, provides an electron source through photoionisation of argon in the region labelled S1, S2, S3 [3]. Electrons are generated in this region at a nominal zero potential through photoionisation with 1.5 meV resolution within ~5 meV of threshold (78.67 nm or 15.764 eV) at the $3p^5(^2P_{3/2})$ 9d resonance at 78.675 nm or ~15.759 eV [51]. This creates photoelectrons with a corresponding energy resolution of ~1.5 meV. The photon beam waist is a few tens of microns and electrons are expelled from the region of photoionisation in a 0.4 V/cm electric field with-

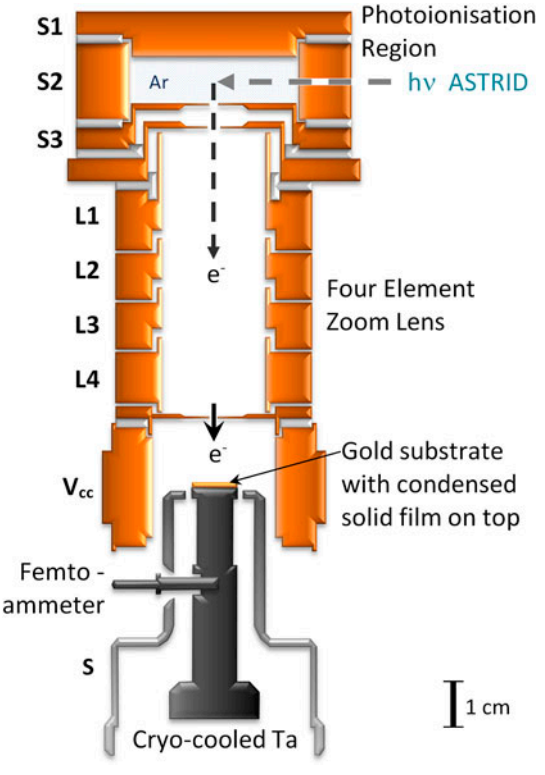

Figure 2. (Colour online) A schematic diagram of the experimental apparatus. Synchrotron radiation (hν ASTRID) with a resolution of 1.5 meV enters a photoionisation source S1, S2, S3 containing argon at a pressure of typically 10^{-4} mbar. Photoelectrons are transported onto condensed solid films at temperatures of 38 K and above. Currents are detected with a Keithley 6340 femtoammeter. L1–L4 constitute a four-element electron lens, V_{cc} is a further focussing element and S is a shield.

out significant loss of energy resolution [3]. The beam of electrons so formed is transported through a 4-element electrostatic lens, L1–L4 (Figure 2) and impinges on the film surface.

Experimental details of the photoionisation source and electron lens system have been described extensively elsewhere, for example in Ref. [3]. Very briefly, the diameter of the electron beam is 2–3 mm depending on the electron energy but naturally acquires a greater opening angle according to the Helmholtz–Lagrange relationship as the electron energy approaches zero. The current at the Au substrate is measured using a femtoammeter (Keithley 6430). All surfaces S1–L4, V_{cc}, and the shield *S*, Figure 2, are spray coated with Acheson Aerodag G graphite to ensure a uniform surface. The apparatus is enclosed in a double mu-metal shield to exclude the magnetic field of the Earth or other stray fields. The electron energy is varied by applying a variable offset potential to the entire electron source with respect to the sample. The zero of energy is taken to correspond to the value of offset potential for which current becomes measurable, that is, 2–3 fA.

2.3. *Substrate characteristics and film preparation*

The base pressure of the system is $\sim 10^{-10}$ mbar. When performing experiments to measure surface potentials the total pressure rises to $\sim 10^{-7}$ mbar when Ar is introduced into the photoionisation region. The gas is of 99.9999% purity and investigations show no evidence of deposition of impurities in the Ar, in the form of molecular films on the gold substrate, arising from many hours exposure to this pressure of Ar. The base temperature of the gold substrate of 38 K is insufficiently low to condense Ar. In addition, without Ar present, surface contamination from background gas or charging of films in the absence of an electron beam could not be detected. A very sensitive check of the lack of contamination, by impurities in Ar or by the background gas, is the stability at the mV level of the surface potential of the gold or of a molecular film, noting that any accumulation of impurities or some source of charge would lead to a readily detectable effect. Experiments on the charging of ice [7] have established that changes in potential at the sample of 1–2 mV may be detected with this system.

Films are prepared under UHV conditions and are laid down from ambient gas on a polycrystalline Au substrate, grain size <100 nm, in the form of a 750 nm thick layer of material on Ta. The substrate is cooled with a He cryo-cooler to temperatures in the range of 38 K upwards and cleaned by heating to 700 K. All recorded values of surface potential are with respect to the clean Au substrate. Standard dosing techniques from the background gas allow the deposition of uniform films of a known number of ML, the latter measured using temperature programmed desorption (TPD). The rate of dosing differed substantially from one species to another, varying between 0.4 ML/min for isoprene to 10.7 ML/min for CF_3Cl normalised to the same nominal background dosing pressure of 5×10^{-8} mbar. Dosing rates were measured to be independent of the temperature at which dosing was performed, that is, the deposition temperature, for the ranges of temperature of interest here. Note that absolute thicknesses of layers in terms of number of ML are known to no better than ±20–30%. Relative values for the same material are, however, generally accurate at the few percent level.

The molecules investigated are not found to decompose on the polycrystalline gold surface at the temperatures employed. Mass spectrometric data associated with TPD data show no trace of any species other than the pure gas with which the surface was dosed. This is in keeping for example with results reported for N_2O on Ag [52].

2.4. *Use of a trochoidal electron monochromator*

Since the spontelectric effect was new and unexpected, it was thought well to detect the characteristic surface potential by a more conventional means than the Ar synchrotron radiation source described above – in case some artefact had been overlooked. For this purpose experiments have also been performed using a trochoidal electron monochromator (TEM) [53], the principle of operation of which has most recently been reviewed in Ref. [54] and which is very widely used in electron scattering experiments. Very briefly, energy selection operates through the electron energy dependence of the physical displacement of an electron beam, generated from a filament, in a crossed electric and magnetic field. Our TEM, not shown in Figure 2, is a miniaturised version that is fitted before the element S1 of the photoionisation source. This element has a 1.8 mm diameter aperture at its centre to allow the passage of electrons from the TEM. The TEM employs an axial magnetic field of $\sim 10^{-3}$ T in our system and the resolution in the beam is estimated from the form of the onset of current at the substrate to be ~150 meV. The energy of the onset of current detection is then determined by the potential of the filament relative to that of the gold substrate.

The TEM enables us to locate current onsets to better than 10 mV, given the high stability with which we are able to run the source at currents of 200 fA and below. TEM data confirmed in detail the results obtained with the photoionisation source for our 'standard' molecule N_2O. Data obtained with the TEM, for example for N_2O films of 71, 142, 213 and 355 ML at 40 K, match those found with the photoionisation source to within a few mV. This demonstrates that there are no unrecognised artefacts associated with use of the less conventional high-resolution photoionisation source.

The TEM also provides a valuable quick look at films. For example, in the periods when synchrotron source ASTRID was not available, we were able to show that both ethyl formate and dihydrofuran were spontelectrics. In addition, the TEM also allows us to use high currents, for example, several picoamps, to observe the removal of the surface potential by electron trapping. Experiments that involve the irradiation of positive going spontelectrics with a sufficient dose of electrons to eliminate the surface potential are described in Section 3.5.

3. Experimental results illustrating detailed properties of spontelectrics

The purpose of this section is to gather together selected data on the spontelectric materials so far detected (Figure 1), that is, N_2O, $CFCl_3$, CF_2Cl_2, CF_3Cl, propane, isopentane, isoprene, toluene, methyl formate, ethyl formate and dihydrofuran. Data are chosen here to illustrate the salient characteristics of the spontelectrics listed in Section 1.1. All data, save raw data for methyl formate and those few for ethyl formate and dihydrofuran, have been reported elsewhere [8–12]. In Section 3.1, we present experimental results showing the variation of surface potentials with film thickness and with temperature of deposition, including the lack of effect of the nature of the substrate. In Section 3.2, data are presented for methyl formate showing the unexpected behaviour that dipole alignment, albeit unstable with time, *increases* with temperature beyond a critical temperature of deposition. In Section 3.3, we describe instances of the instability of the spontelectric field with time in more detail. In Section 3.4, Curie points are shown for a variety of species, in Section 3.5 the removal of the spontelectric potential by irradiation with large electron doses is described and in Section 3.6 some preliminary data for

Table 1. Data for all known spontelectrics at 40 K (except where specified for CF_2Cl_2 and $CFCl_3$) in terms of mV per ML.

Molecule	Temperature/K	mV/ML	Electric field V/m	Degree of dipole alignment	Gas phase dipole moment/D
Propane	40	−0.72 and −4.77	–	–	0.08
Isopentane	40	−7.8	–	–	0.13
N_2O	40	+32	9.72×10^7	0.124	0.167
Isoprene	40	+35	–	–	0.25
Toluene	40	+6.5	–	–	0.385
CF_3Cl	40	−11.6	-4.25×10^7	0.052	0.500
CF_2Cl_2	45	−3.97	-1.43×10^7	0.042	0.510
$CFCl_3$	43	−1.33	-0.532×10^7	0.031	0.45
Methyl formate	40	5.78	2.21×10^7	0.0185	1.766
Ethyl formate	40	∼20 mV/L	–	–	1.98
2,5-Dihydrofuran	40	2.7 mV/L	–	–	1.75

For ethyl formate and 2,5-dihydrofuran, results are expressed as mV per Langmuir since TPD data are not available for these species. Also shown are gas-phase dipole moments and, where these have been derived, spontelectric fields within films and the corresponding degree of dipole alignment; see Section 4.

a spontelectric heterostructure giving rise to a nano-well consisting of N_2O and isopentane are presented.

The assumption is made in the subsequent discussion of the spontelectric effect that the solid films described here are amorphous rather than crystalline. This is for two reasons: (i) films laid down by vacuum deposition at low temperature, under the conditions described here, tend to be amorphous and (ii) the properties of crystalline materials are dictated by their crystal structure and therefore should show little change over a range of temperature of deposition for which the material experiences no change of phase. By contrast, it is characteristic of spontelectric films that small changes in temperature cause significant changes in the molecular order, with electric fields within the material changing by a factor of 5–10 over a temperature range of a few tens of K or less. Note that the term amorphous does not imply a random structure, since films exhibit dipole alignment.

Data for all known spontelectrics deposited at 40 K, save for CF_2Cl_2 and $CFCl_3$, respectively, at 45 and 43 K, are shown in Table 1.

3.1. *Spontaneous surface potential data*

Positive going surface potentials formed on films of N_2O, isoprene and toluene for a variety of deposition temperatures are shown in Figures 3–5 respectively. Negative surface potentials are illustrated in Figures 6–8 for films of isopentane, CF_3Cl and CF_2Cl_2. All surface potentials are relative to the gold surface potential.

Data in Figures 3–8 show a linear dependence of potential on film thickness, which is taken as good evidence for the presence of a constant electric field within the film. This in turn indicates that there is negligible net charge stored within the film. Note that layers of a minimum thickness of 50–100 ML may be required to establish the spontelectric effect, illustrated in the case of isoprene laid down at 70 K (Figure 4) or toluene laid down at 75 or 90 K (see inset to Figure 5).

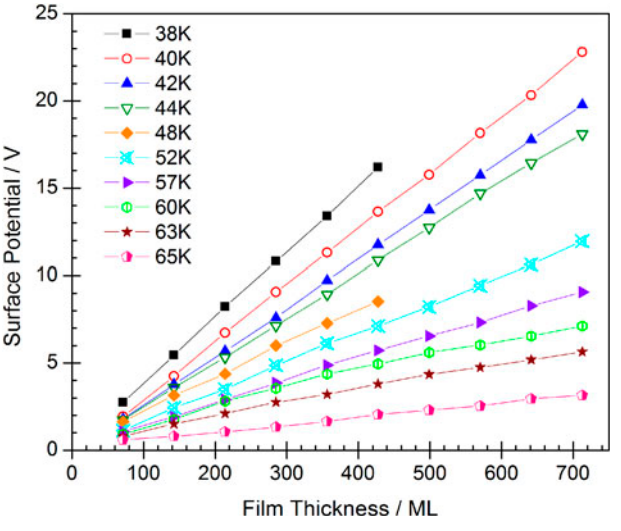

Figure 3. (Colour online) Surface potentials measured for films of N_2O as a function of thickness in ML laid down at ten different deposition temperatures.

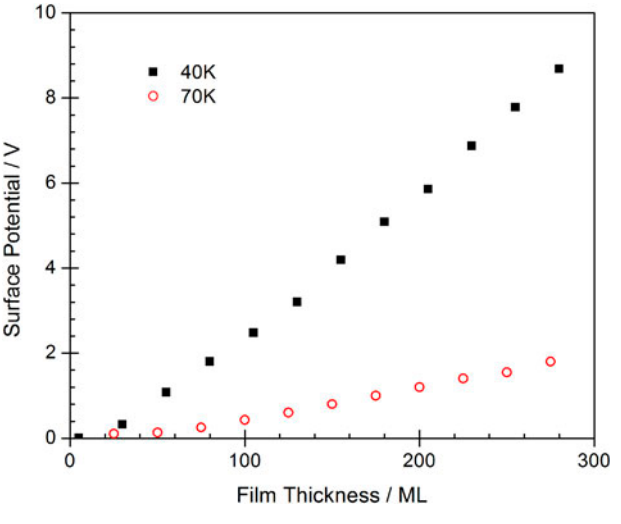

Figure 4. (Colour online) The variation with film thickness (ML) of the surface potential on films of isoprene deposited at 40 K and 70 K.

Data in these figures illustrate that the spontelectric effect is strongly dependent on the temperature of deposition. Figures 7 and 8 for CF_3Cl and CF_2Cl_2 illustrate that at sufficiently high deposition temperatures, of 55 K and 75 K, respectively, no surface potential is observed. Figure 9 shows further data for N_2O demonstrating that very high surface potentials, in this case of 38 V, can be readily achieved. This limit was set only by the practical consideration

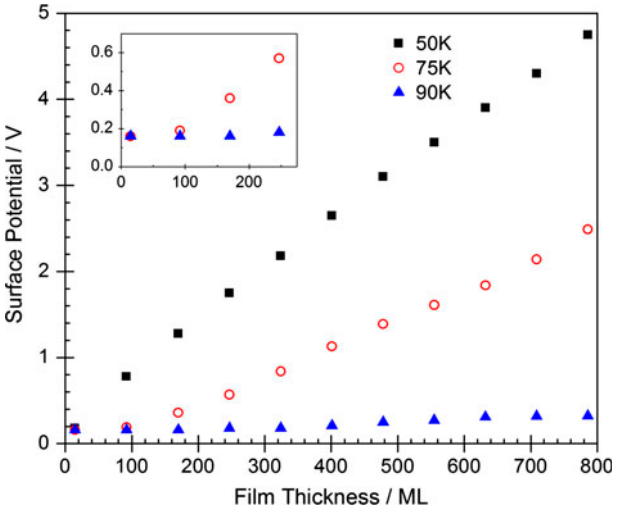

Figure 5. (Colour online) The variation with film thickness (ML) of the surface potential on films of toluene deposited at 50, 75 and 90 K. The inset shows the behaviour at low coverage for 75 and 90 K.

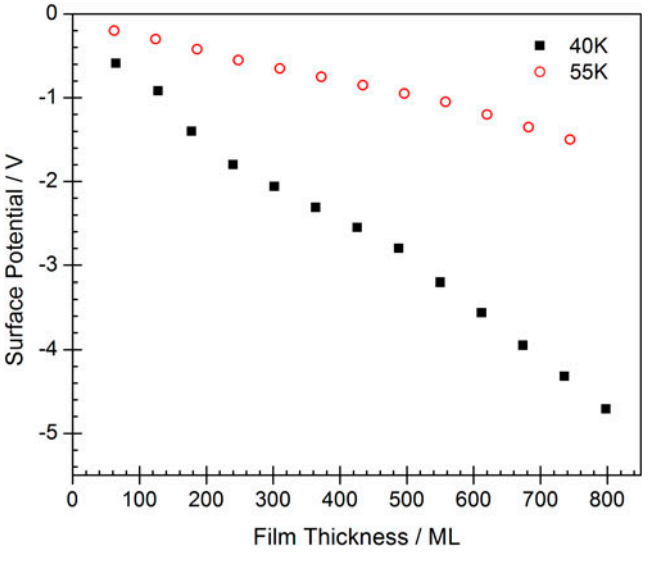

Figure 6. (Colour online) The variation with film thickness (ML) of the surface potential on films of isopentane deposited at 40 K and 55 K. The departure from linearity at 40 K is an experimental artefact due to instability in the dosing rate of isopentane.

that there was a risk of damage to the femtoammeter (see caption to Figure 2) if it were floated to higher potential.

An important general point, mentioned in the introduction, is that the nature of the surface upon which spontelectric films are deposited has little or no bearing on the values of surface

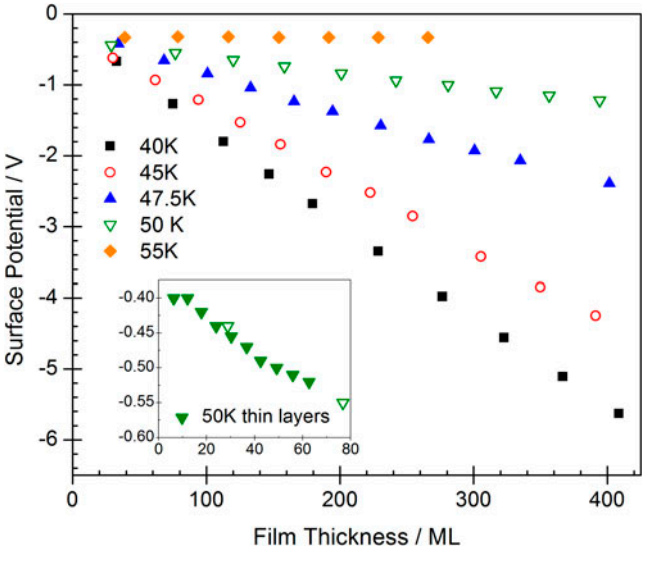

Figure 7. (Colour online) Surface potentials measured for films of CF_3Cl as a function of thickness in ML laid down at five different deposition temperatures. 55 K data are included to show the absence of the spontelectric effect. Note the small thickness independent surface potential at 55 K due to surface dipoles referred to in Section 1.2.1. The inset shows data at 50 K for a lower rate of deposition (see text).

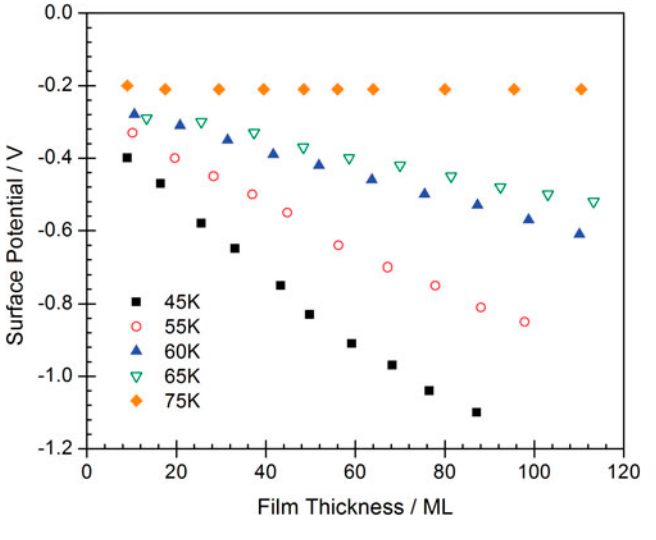

Figure 8. (Colour online) Surface potentials measured for films of CF_2Cl_2 as a function of thickness in ML laid down at five different deposition temperatures; 75 K data are included to show the absence of the spontelectric effect.

potential. Thus all results presented here, so far as we have presently ascertained, are independent of the fact that spontelectric materials are laid down upon a Au surface. This reinforces the point that the spontelectric effect is essentially a bulk effect involving the

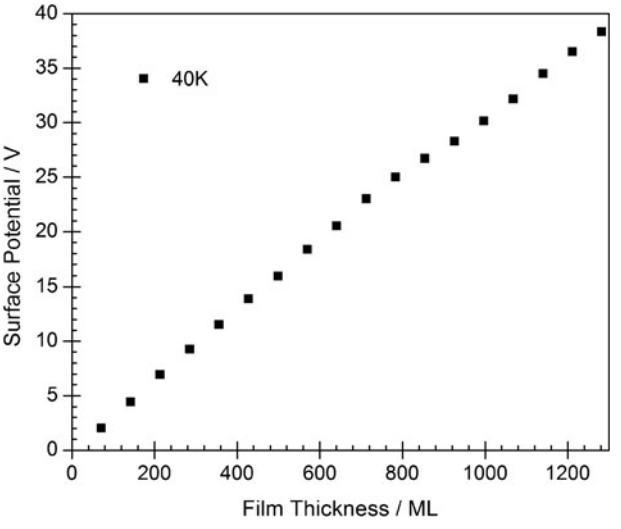

Figure 9. Surface potentials measured for films of N_2O deposited at 40 K as a function of thickness in ML extended to high potentials.

long-range action of the electric field within the film. Experiments that exemplify this involve (i) depositing first a layer of Xe on Au and then a layer of N_2O and (ii) depositing composite heterostructures of spontelectrics.

Turning first to (i), experiments have been performed involving 1 ML of Xe with N_2O deposited on top at 58 K, the same but with 50 ML of Xe, the same but at 63 K and 15 ML of Xe and the same but at 65 K and 5 ML of Xe. No significant differences at the mV level were found for measured surface potentials on N_2O films compared with N_2O films laid down in the absence of Xe films at these temperatures. With reference to point (ii), a single example of a heterostructure is given in Section 3.6 which again exemplifies the independence of the magnitude of the spontelectric field on the underlying material, at any rate for sufficiently thick films.

3.2. *The anomalous case of methyl formate, $HCOOCH_3$*

Data for methyl formate for a variety of temperatures between 40 and 89 K, selected for clarity of presentation, are shown in Figures 10–12. We ignore for the present the curvature of some of the data for surface potential vs. film thickness, to which we return in Section 3.3, and concentrate on the initial slopes. These slopes give the electric field within the film as initially laid down. It is evident that the electric field in methyl formate films at first decreases with temperature of deposition, as in other spontelectrics. However, at greater temperature, around 78–80 K, the electric field begins to rise quite steeply. This may be seen in Figure 12 in which the initial gradient increases sharply between deposition temperatures of 80 K and 88 K. This behaviour will be discussed in detail in Section 4.2.3.

Data for ethyl formate and dihydrofuran are shown in Figures 13 and 14. The drop in slope of surface potential vs. dose of material, where this slope is a measure of electric field,

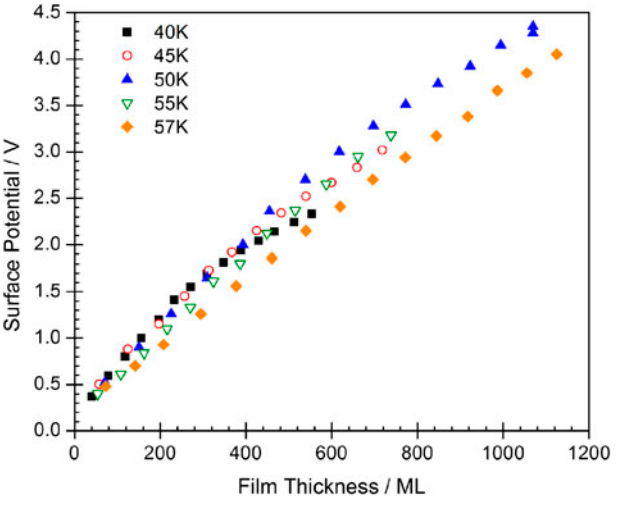

Figure 10. (Colour online) Surface potentials measured for films of methyl formate, $HCOOCH_3$, as a function of thickness in ML for the deposition temperature range 45–57 K.

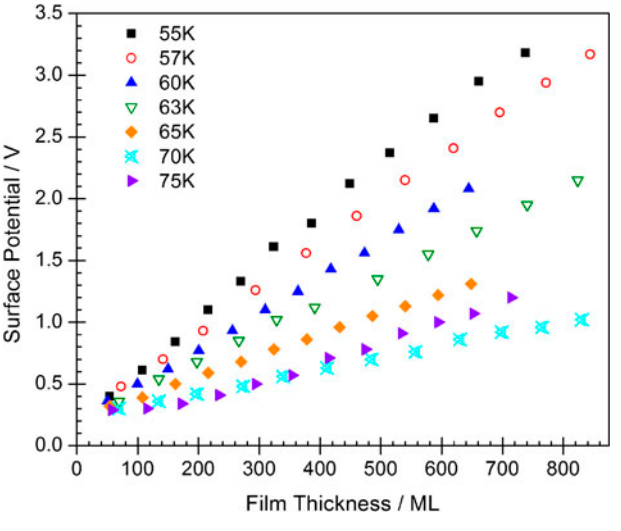

Figure 11. (Colour online) Surface potentials measured for films of methyl formate, $HCOOCH_3$, as a function of thickness in ML for the deposition temperature range 55–75 K.

between 40 K and 60 K for ethyl formate or 40 K and 70 K for dihydrofuran is not especially marked when compared with other spontelectric materials. This may be indicative of qualitatively similar behaviour to that seen in methyl formate in Figures 10–12. Further data are required to explore this. Ethyl formate is, however, clearly distinct from methyl formate in that deposition at 80 K creates films that show no spontelectric effect.

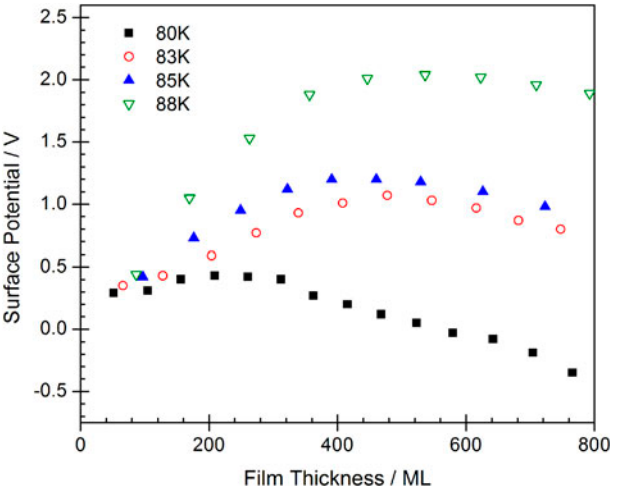

Figure 12. (Colour online) Surface potentials measured for films of methyl formate, $HCOOCH_3$, as a function of thickness in ML for the deposition temperature range 80–88 K. The decay of the spontelectric effect for higher coverage may be attributed to the instability of the effect with time rather than an effect of thicker layers of material; see Section 3.3.

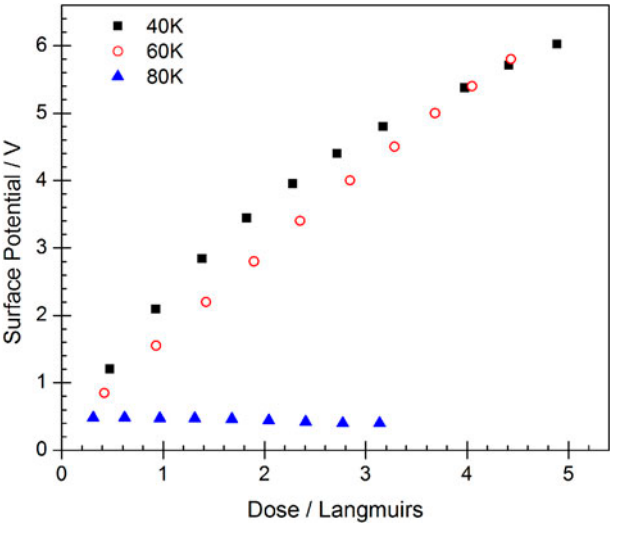

Figure 13. (Colour online) Surface potentials measured for films of ethyl formate, $HCOOC_2H_5$, as a function of thickness in Langmuirs for the deposition temperatures 40 K and 60 K. Data at 80 K are included to illustrate that this temperature is too high to create a spontelectric film for ethyl formate, in contrast to methyl formate (see Figure 12). Data are shown in Langmuirs in the absence of TPD data for this species.

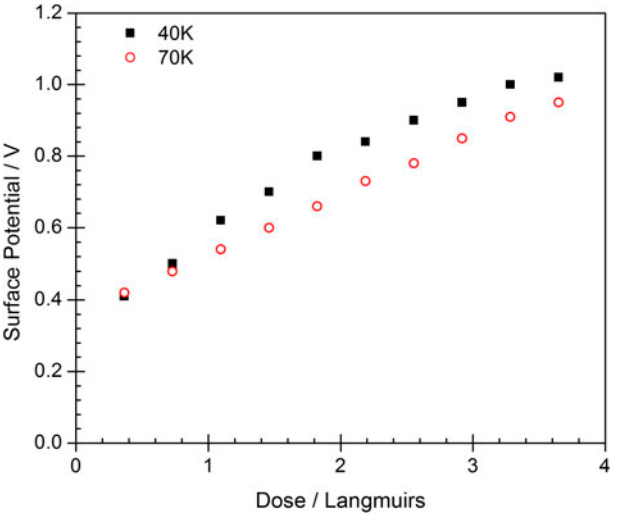

Figure 14. (Colour online) Surface potentials measured for films of dihydrofuran, as a function of thickness in Langmuirs for the deposition temperatures 40 K and 70 K. Data are shown in Langmuirs in the absence of TPD data for this species.

3.3. *Temporal variation of the spontelectric field*

Almost all spontelectric films show temporal stability over a period of at least several hours. In one experiment, a 40 K film of N_2O was allowed to stand overnight. The measured surface potential was unchanged within experimental error, that is, 2–3 mV. Risk of contamination makes tests over longer periods of time difficult.

Exceptionally, however, the variation of the spontelectric potential with layer thickness is not linear but rather tends to show a lesser potential than the initial linear slope suggests or altogether to reverse the trend of increasing surface potential with film thickness. An example of the latter may be found in Figure 12 for methyl formate. This is interpreted as a decay of the spontelectric structure with time and may be observed for some ranges of deposition temperature of propane, methyl formate, ethyl formate, dihydrofuran and $CFCl_3$. Data for $CFCl_3$ are shown in Figure 15 illustrating the abrupt change of behaviour between deposition temperatures of 46 K and 50 K. Direct decay with time is illustrated for this species deposited at 50 K by data in Figure 16 showing a (near) linear decay from a value of -0.44 V over a period of 3 hours towards the value of ~ -0.27 V relative to clean gold associated with a single monolayer of $CFCl_3$. The latter figure represents the surface dipole effect described in Section 1.2.1. Data in Figure 16 support the attribution of departure from linearity of surface potential with film thickness to temporal decay. The trait of curvature of the surface potential with film thickness, seen for example in Figure 15, contains an experimental artefact relating to the time involved in acquiring the surface potential for each layer thickness. This time is typically about 10 min but is not controlled in the experiment.

Turning to methyl formate, the decay of the spontelectric potential is greatest at higher temperatures $\gtrsim$80 K as illustrated in Figure 12. There is also a low temperature range

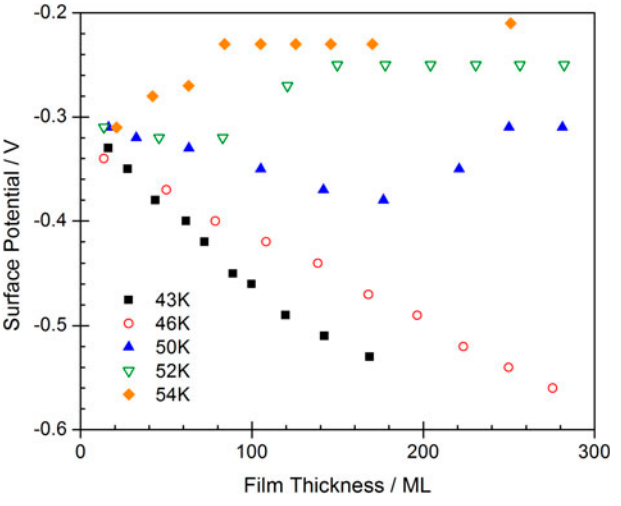

Figure 15. (Colour online) Surface potentials measured for films of $CFCl_3$ as a function of thickness in ML laid down at five different deposition temperatures. These data illustrate temporal decay of the spontelectric effect for deposition temperatures $\geqslant 50$ K (see text).

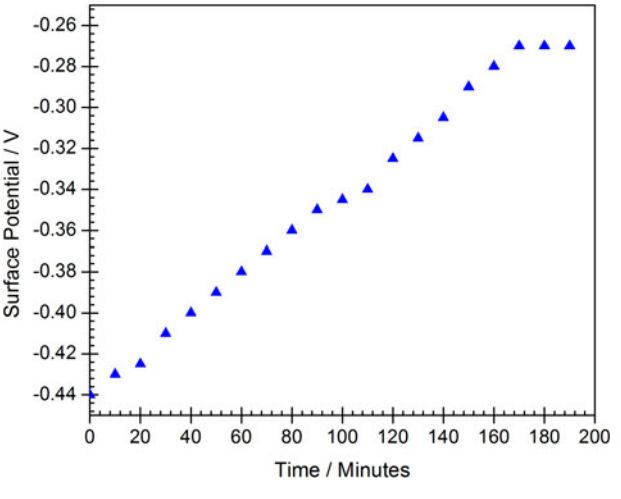

Figure 16. The temporal decay of the surface potential of a film of $CFCl_3$ of 250 ML deposited at 50 K.

between 40 K and ~55 K for which curvature of the observed spontelectric field vs. layer thickness is found and here temporal instability tends to decrease as temperature of deposition is increased. The stability of methyl formate films above 55 K and instability below suggests a structural change in methyl formate at around this temperature, an interpretation that is borne out by Curie point data presented in Section 3.4.

3.4. *The temperature-induced decay of spontelectric fields: robustness of the spontelectric structure and the presence of Curie points*

What takes place when a spontelectric film is deposited at a low temperature and then heated? As we have noted in the introduction, spontelectric films are robust to temperature stress. For example, a N_2O film of 360 ML thickness was laid down at 38 K and heated, with measurements taken every 3–4 K to just below the evaporation point at 75 K. The potential dropped by only 510 meV at 75 K compared with the value at 38 K. This may be compared with data in Figure 3 where results for the relaxed state show a drop of 11.95 V between 38 and 65 K, where these temperatures refer to temperatures of film deposition. Evidently, the dipole aligned structure shows powerful rigidity and remains in place despite the substantial electromechanical stress that this implies.

In general if heating is continued, a critical temperature is reached at which the spontelectric effect decays with various degrees of abruptness depending on the material. Thus it is a particular characteristic of spontelectric films that, through warming of the film, dipole alignment disappears at a specific temperature or range of temperatures, while falling little at lower temperatures. Material is meanwhile not evaporated from the surface and the film survives but is no longer aligned. By analogy with ferromagnetism, the critical temperature is referred to as a Curie point. The effect is also analogous to loss of spontaneous polarisation in piezoelectric materials.

All materials investigated show characteristic Curie points, with the possible exception of N_2O for which the sublimation temperature and the Curie point cannot be experimentally separated. The example of isoprene is given in Figure 17. The film of 300 ML was heated from 40 K to 82 K over a period of 160 min showing an abrupt change in potential around 70 K terminating at 80 K. In this connection isoprene begins to evaporate from the gold substrate only above 105 K. These data also serve once more to illustrate the robustness of the

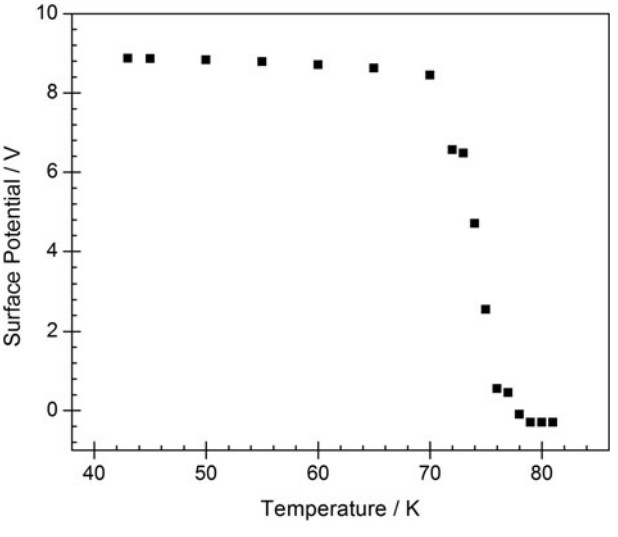

Figure 17. The variation of the surface potential of a 300 ML film of isoprene laid down at 40 K and warmed to 82 K showing a Curie point.

spontelectric effect: the surface potential remains almost constant up to 70 K, whereas Figure 4 shows that a drop of more than 6 V would be expected. We also note that for similar rates of heating, the Curie effect can be very sharp in temperature, as illustrated by Figure 18 for $CFCl_3$ where decay takes place over 1–2 K, or relatively broad, as illustrated in Figure 19 for

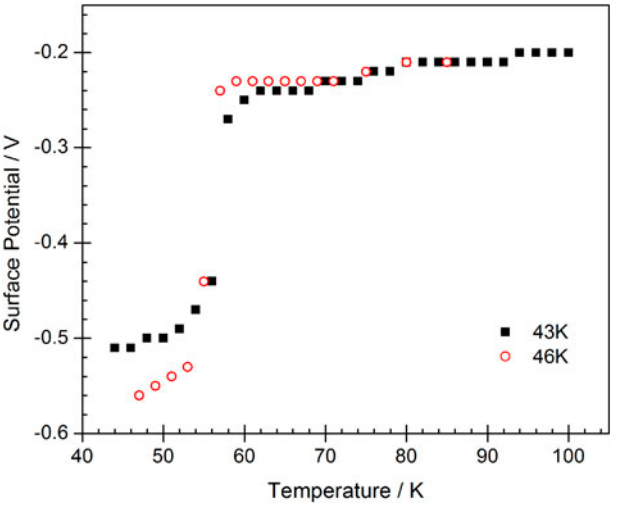

Figure 18. (Colour online) $CFCl_3$: black points: the variation with temperature of the surface potential of a 120 ML film of $CFCl_3$ laid down at 43 K and heated to 100 K. Red points: the same for a 250 ML film of $CFCl_3$ laid down at 46 K and heated to 84 K.

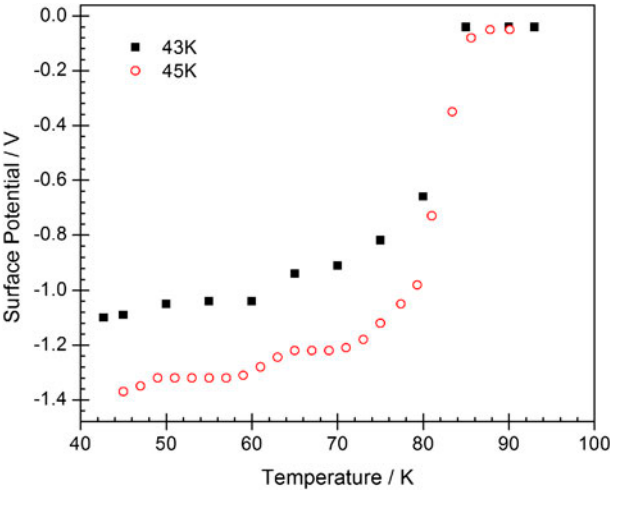

Figure 19. (Colour online) CF_2Cl_2: black points (upper curve): the variation of the surface potential of a 90 ML film of CF_2Cl_2 laid down at 43 K and heated to 95 K showing a Curie point. Red points (lower curve): the variation of the surface potential of a 120 ML film of CF_2Cl_2 laid down at 45 K and heated to 95 K.

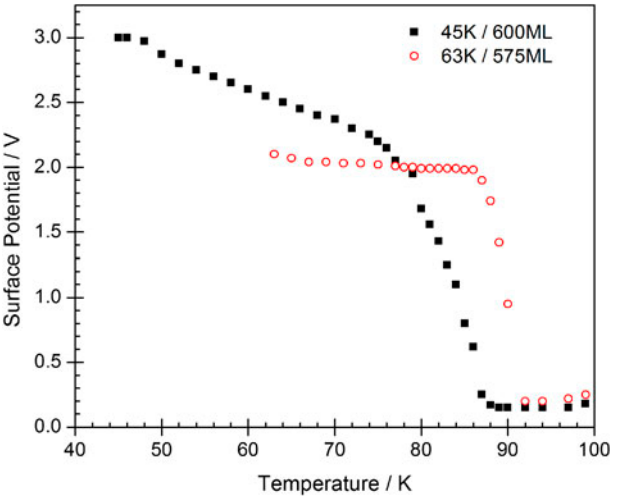

Figure 20. (Colour online) Methyl formate: values of the surface potential as the temperature of films deposited at 45 K (black squares) and 63 K (red circles) is slowly raised, showing different Curie temperatures (see text).

CF_2Cl_2 where decay takes place over 10–15 K. Errors in experimental values of surface potential are 2–3 mV and of the temperature are ±1 K as throughout.

If the assumption is made that the Curie point is characteristic of a distinct phase of the material, then Curie data can be used to exemplify the formation of different phases when material is laid down at different temperatures. This is illustrated by Curie data for methyl formate in Figure 20 where data for films deposited at 45 K and 63 K are compared. The former show a Curie point at 82 K, whereas the latter shows a value of 90 K. These data suggest a structural change in methyl formate at a deposition temperature between 45 K and 63 K. This is in keeping with the instability in time associated with lower temperature deposition, such as 45 K, and the stability associated with intermediate temperature depositions, such as 63 K, shown in Figure 11. The temporal decay of methyl formate films deposited at 45 K, referred to in Section 3.3, may also be seen in Figure 10, through the curvature of the surface potential vs. film thickness data.

Further evidence of structural complexity may be gleaned from Figure 19 showing the Curie point for CF_2Cl_2. The drop in the spontelectric potential in these data around 60–65 K suggested by results shown in the upper curve in Figure 19 for a film laid down at 43 K taken with 5 K steps, is confirmed by data in an experiment conducted with 2 K steps, in the lower curve (for a film laid down at 45 K). These data suggest therefore that solid CF_2Cl_2 may form two spontelectric configurations which transform one into the other at >60 K. Alternatively, there may be two co-existent configurations with the conversion of one into the other at >60 K.

3.5. *Removal of the surface potential and charging of surfaces by electron irradiation*

A positive potential on the surface of the film of a spontelectric requires that charge, free or bound, be present on the surface. At the surface–vacuum interface, the protrusion of the

positive moiety of N_2O results in a charge density on the surface and gives rise to polarisation and a positive voltage. Thus, as described in Section 1.3, irradiation of the surface of a positive-going spontelectric with a sufficient dose of electrons must lead to a reduction of the surface potential. Indeed, it could lead to the complete removal of the spontelectric potential, and this was cited in Section 1.3 as the reason why the spontelectric effect has not been observed in earlier work.

To establish this phenomenon and give additional credence to our hypothesis of the origin of the spontelectric effect, we irradiated a surface of a 540 ML N_2O film, prepared at 60 K showing a spontelectric potential of 4.8 V positive, for a period of 1800 s with a current of 200 fA at a nominal energy of 300 meV [8]. This yielded a total dose equivalent to $\sim 5.1 \times 10^{-5}$ C/m^2. The surface was observed to shift 200 mV less positive. The charge delivered is equivalent to 11.7% of the total spontaneous polarisation. Therefore, the maximum possible shift should be 11.7% of the total surface potential of 4.8 V for this film, that is, 560 mV, if all charge accumulates at the surface and is sufficiently mobile to neutralise the surface polarisation. Electrons at 300 meV penetrate the film but encounter the band gap and are therefore unable to reach the film–metal interface. They are multiply scattered and return towards the film–vacuum interface. At the surface, they are attracted by the positive charge and partially neutralise it. Electrons destroyed the spontelectric potential with an apparent 30% efficiency in this example, although this figure may be higher due to the fact that the electron beam does not match in diameter that of the sample.

Experiments have also been performed using the TEM (Section 2.4) to irradiate a 355 ML sample of N_2O laid down at 60 K with ~13 pA for a total of 45 min, equivalent to a total charge of 3.5×10^{-8} C. The initial spontelectric potential of 3 V was completely removed. This result corroborates the explanation in Section 1.3 of why the phenomenon of spontaneous polarisation has not been observed in numerous earlier experiments of other groups in which currents were generally nA and times of irradiation a few to tens of seconds [55].

Materials may in general charge negative on irradiation by electron beams and this may introduce systematic errors into our data. The extent of charging may be measured by repeated scanning of the electron current as a function of potential for any chosen film thickness and observing any shift in the onset [7]. Such a shift would represent the accumulation of a negative potential in the case of negative-going spontelectrics and artificially enhance the measured spontelectric effect, introducing systematic errors into the data. The effect would reduce the spontelectric effect in positive going species.

Effects of charging for N_2O, isopentane or isoprene are at the level of <10 meV for 100 s of irradiation at 200 fA over an incident electron energy range of 0–500 meV. For propane, we estimate that charging leads to an overestimate of negative values shown in Table 1 by ~5% in the case of the lower figure of −0.72 mV/ML and <1% for the figure of −4.77 mV/ML. The error for films of toluene, which charge appreciably, lead to an overestimate by 9% and this is included in the value given in Table 1. For the three chlorofluorocarbons, charging yields an overestimate of the spontelectric potential of $\leqslant$2%.

3.6. *Tailoring electric fields through fabrication of a heterostructure*

Data are shown here which demonstrate that it is possible to tailor a set of potentials by depositing films one upon the other to form a heterostructure. In the example given, a

spontelectric that possesses a positive surface potential is combined with one that possesses a negative potential to create a potential well. On the basis of experimental data for the individual species, it is known that at 40 K 33 ML of N_2O gives +800 mV and deposition of 183 ML of isopentane gives −800 mV. Thus, deposition of N_2O and subsequent deposition of isopentane should in principle create a net zero polarisation potential on the surface and yield an asymmetric triangular well of depth 800 meV. This is based on the assumptions that there is no significant interpenetration of these two layers and that the electrical behaviour of one is unaffected by the other and that a well-defined boundary can be formed.

Remarkably, this simple prescription works exactly as described. A 33 ML film of N_2O was first prepared at 40 K on gold forming a positive surface potential of 800 mV. As isopentane was dosed in stages on top of the N_2O, the reduction in the 800 mV potential to zero could be followed, a value achieved when 183 ML of isoprene had been formed, as predicted from the behaviour of the independent layers. A further layer of N_2O was added raising the potential once more to 800 mV with a subsequent layer of isopentane restoring the potential to zero. There was no necessity for, say, a Xe spacer between the two species and the development of the isopentane potential proceeded as on deposition on polycrystalline Au. This reinforces the conclusion that bulk spontelectric behaviour is independent of the nature of the substrate, as set out in Section 3.1. Very recent work on a variety of heterostructures, however, shows that the electric field in the film in the neighbourhood of the junction of the two spontelectrics is in fact modified in general from bulk values [56], but settles down to the unperturbed value when a sufficiently thick film of typically 50–100 ML is laid down.

4. Understanding the results

The overall impression left by the data presented in the Section 3 is there is a mass of information, largely unintelligible except in the broadest terms – and some data not even in those terms, such as the anomalous rise in electric field with increasing deposition temperature for methyl formate. The purpose of the current section is to summarise our present imperfect understanding of the spontelectric effect and shed some light on the physics that causes it.

Following the conclusion drawn in Section 1 that spontelectrics represent a new phenomenon in solid-state physics, many questions spring to the mind of an investigating scientist, just as they must have done when Rochelle Salt was investigated and the terms ‘piezoelectric’ and ‘ferroelectric’ were first coined. Here we narrow these questions down to a single question, what is the nature of the interactions that give rise to a powerful electric field within spontelectrics? We attempt to give insight into this by focussing wholly upon the variation of the spontelectric field with deposition temperature. Thus, all temporal effects (Section 3.3) and Curie points (Section 3.4), interesting as they may be, are excluded.

4.1. *A theoretical model*

There is a host of theoretical work, based on Ising lattice models [57], devoted to phenomena for both ferromagnetic and ferroelectric materials, with which, as noted in Section 1.2.4, the

present polarised phase has aspects in common. Lattice systems in which electric moment interactions play a fundamental role are treated for example in Ref. [58]. In common with this and much other work, a lattice model is adopted here using a Hamiltonian that is composed of a long-range dipole–dipole interaction and a term which essentially frustrates the attempt of the dipoles to align. A term is also included which represents the energy associated with the interaction of the electric field created through dipole alignment with the dipoles themselves. The system is non-linear and non-local since alignment of dipoles creates the field and the field itself creates dipole alignment. Thus, all components of the film communicate over all ranges. The film, in the absence of insurmountable barriers, settles down to a stable configuration corresponding to a balance between both short-range and infinite-range interactions, which together lead to some degree of order, and thermal motion, which leads to disorder. This concept of dipole–dipole ordering countered by a tendency to disorder through thermal motion follows naturally from the strong temperature dependence of the spontelectric field on deposition temperature, illustrated for example in Figure 3 for N_2O. The control parameter of the physics is therefore the energy associated with the interaction of the dipole with the local electric field divided by the thermal energy.

In our experiments, we can vary only the temperature of the substrate on which the material is deposited, the temperature after deposition, the thickness of the layer formed and the nature of the substrate on which the film is deposited. How therefore to proceed to an understanding of what gives rise to the spontelectric effect? Our hypothesis, as we have mentioned earlier, is that the net macroscopic polarisation, which we observe in terms of an inferred electric field within spontelectric films, is due to partial alignment of dipoles within the film. We assert further that these dipoles are those associated with individual molecules rather than dipolar zones of large molecular aggregates, as suggested for example in ferroelectric glasses [59]. Thus, we conjure up the rather counter-intuitive image of dipolar species falling from the gas phase and condensing into configurations with the positive ends of dipoles, say, having no strong aversion, on average, to sitting closer to other positive ends than local electrostatics would dictate. This counter-intuitive configuration is essential if there is to be net order in the system and an order which leads to dipole alignment. It arises, as we have indicated previously, because this configuration creates a macroscopic electric field in the system which itself tends to orient dipoles head to head and tail to tail.

At this stage we introduce the concept of the degree of dipole alignment. If we consider any one dipolar species in the solid, the dipole will be pointing in some direction. We define the degree of dipole alignment of the ensemble as a whole as the average component of the dipole pointing in the direction in which we have measured the electric field, the *z*-direction, that is, perpendicular to the plane of the film, divided by the total dipole moment of the molecule. Immediately, we hit a snag. Is this *z*-component of the dipole flapping about in the electrical breeze, so to speak, or is it frozen into position? In the first, we should consider a time average value of the direction of any species, whereas in the second, an average over a very large number of dipoles for each of which the direction is rigidly fixed. We do not know which is correct, a time average or a space average. So we choose to make no difference between a space and a time average, consistent with the use of thermodynamic arguments below. This remains rather unsatisfactory if we seek to visualise the nature of spontelectric solids.

At all events, if we agree that dipoles can be to some degree ordered, then this yields a macroscopic polarisation and associated electric field. That is not all, though. A crucial point,

already alluded to, is that the electric field arising from ordering of the dipoles creates a field that tends to align the dipoles themselves. The system therefore experiences positive feedback: the more the alignment, the more the field, thus the more the alignment and so on. A characteristic of such feedback systems is that small natural fluctuations can feed an initially disordered system and spontaneously create order. Here a disordered system achieves macroscopic order by dipoles talking to each other and conversing at effectively infinite range through a self-generated electric field. This, we postulate, is how films can be so readily spontelectric.

The essential idea is that if dipoles are aligned then either the positive or negative end will predominate at the film–vacuum interface and correspondingly the negative or positive end will predominate at the film–substrate interface. This leads to a polarisation of the medium with the result that a constant electric field will be found within the film. Note that the presence of charge in the bulk would create a varying electric field, inconsistent with observations. The spontelectric effect is a concerted bulk effect and in general requires some minimum film thickness to become established. Data in Figures 4 and 5 have already been cited in which layers of a minimum thickness of 50–100 ML are required to establish an observable spontelectric effect.

In the otherwise amorphous, but partially ordered array of dipolar species, interactions occur through forces involving dipole–dipole interactions (and in principle higher poles), static polarisation and London dispersion forces. There may also be significant covalent overlap, for example, in N_2O for which dimers and larger clusters are known to form in the gas phase [60,61]. Since we are ignorant of local details of these forces and accompanying structure, we adopt a mean field model in which we consider an average dipole in an average environment. The mean field model is embodied in the statement that the dipole in the *i*th layer, at some angle to the normal, *z*, may be equated to the average dipole at all sites and all angles. One result of the adoption of this model is that no spatial information can be extracted; specifically the model cannot by itself inform us of the presence or absence of domains or isolated areas showing alignment of dipoles [8,59]. The association of dipoles with individual molecules is useful for the purposes of visualisation, but the model does not require this. Rather it deals in dipolar units without specification of what these units are. We are of course still left with an image of dipoles either fixed in space residing individually at a variety of angles, yielding a space average, or undergoing hindered oscillation in a constraining electric field creating a time average. We continue with the image of individual molecules rather than dipolar domains.

If one considers a specific molecule in the film, all other molecules contribute to a local field acting on that molecule. This local field may be conveniently divided into two terms. The first is the term that is present even in the absence of the spontelectric effect and therefore describes any amorphous or so-called glassy system. We refer to this term as the 'symmetric' term since the net field is zero when averaged over the whole film. The second term is the measured field that arises through macroscopic spontaneous dipole alignment. When the film is heated above the Curie point, macroscopic dipole alignment is removed and only the first term survives. This survival arises since *local* dipole alignment, formed on condensation of the film, may be frozen into the system at any temperature below the sublimation point. However, as we have mentioned, the sum of such fields vanishes when averaged over the entire ensemble [62].

The first term, describing the local field, may be formulated in different ways and is described in textbooks [41,63] generally in reference to a particular local lattice symmetry, for example cubic symmetry in the references mentioned. In the case of spontelectrics, a different description is necessary since there is no local symmetry. Moreover, the local field does not involve any external field from external charges [63]. There is therefore no net a priori macroscopic polarisation artificially imposed upon the system. In view of the strictures visited upon the 'standard' theoretical evaluation of the local field, outlined in two sections of Ref. [41] under the titles of the 'Fallacy of the Clausius–Mossoti picture' and the 'Fallacy of defining polarisation via the charge distribution', we choose here simply to postulate that there exists a local symmetric field, as defined previously. The functional form of the local field remains unspecified save that we split the field into two parts, that which is associated with polarisation, dispersion and covalent forces and that which is associated with dipole–dipole interactions. This inclusion in the local field of a term explicitly dependent on dipole–dipole interactions is a crucial step in reproducing spontelectric behaviour. Without it, it is not possible to reproduce either the steeply dependent behaviour of the spontelectric field on deposition temperature (e.g. Figure 3 for N_2O and Sections 4.2.1 and 4.2.2) or the anomalous behaviour of methyl formate (Section 4.2.3).

The dipole–dipole contribution to the local symmetric field is represented as follows. The z-component of the average dipole averages to a non-zero quantity, $\langle\mu_z\rangle$, in a spontelectric film. Note that $\langle\mu_z\rangle$ is, however, zero when such a film is heated to beyond the Curie temperature. The x- and y-components in the plane of the film average to zero under all conditions by symmetry. The average degree of dipole alignment is defined as the direction cosine of μ and $\langle\mu_z\rangle$, that is, $\langle\mu_z\rangle/\mu$, where μ is the dipole of the molecule in its environment in the amorphous solid. Turning to dipole–dipole interactions, these include contributions from dipole–dipole forces, dipole-image charge forces and associated polarisation interactions. These interactions share the common feature that they have an angular dependence governed by $\cos^2\theta$, that is by $(\langle\mu_z\rangle/\mu)^2$, a dependence which includes arrays of dipoles and extended dipoles [64–66]. The full local symmetric field may then be written as $\langle E_{\rm sym}\rangle[1+\zeta(\langle\mu_z\rangle/\mu)^2]$. Note that this remains symmetrical to the orientation of the dipole in the $+z$ or $-z$ direction. Both $\langle E_{\rm sym}\rangle$ and ζ are parameters whose values are unknown and have to be obtained by fitting to experimental data.

To bring this more to life, which of the two terms in this symmetric part of the field is the more important in real spontelectrics, $\langle E_{\rm sym}\rangle$ or $\langle E_{\rm sym}\rangle\zeta(\langle\mu_z\rangle/\mu)^2$? From subsequent fitting to experimental data, Section 4.2, for the three chlorofluorocarbons for films deposited at 45 K for CF_3Cl and CF_2Cl_2 and 46 K for $CFCl_3$, values of $\langle E_{\rm sym}\rangle$ are respectively 6.96×10^7 V/m, 7.0×10^7 V/m and 1.05×10^8 V/m. For comparison $\langle E_{\rm sym}\rangle\zeta(\langle\mu_z\rangle/\mu)^2$ equals 5.6×10^7 V/m, 1.1×10^8 V/m and 2.6×10^8 V/m (see Table 2). Thus the terms $\langle E_{\rm sym}\rangle$ and $\langle E_{\rm sym}\rangle\zeta(\langle\mu_z\rangle/\mu)^2$ are of similar value for these species at this temperature. A similar result is found for N_2O at (say) 40 K. However, for methyl formate at 50 K, the dipole term, $\langle E_{\rm sym}\rangle\zeta(\langle\mu_z\rangle/\mu)^2$, is five times larger than $\langle E_{\rm sym}\rangle$. At higher temperatures, however, the first term, $\langle E_{\rm sym}\rangle$, tends naturally to dominate since the degree of dipole alignment is reduced. Thus for CF_2Cl_2 at 65 K, $\langle E_{\rm sym}\rangle\zeta(\langle\mu_z\rangle/\mu)^2$ is only $\sim$13% of $\langle E_{\rm sym}\rangle$ and for methyl formate the ratio of $\langle E_{\rm sym}\rangle\zeta(\langle\mu_z\rangle/\mu)^2$ to $\langle E_{\rm sym}\rangle$ (or of $\zeta(\langle\mu_z\rangle/\mu)^2$ to unity) falls from 5 at 50 K, as just noted, to 0.1 at 75 K. In answer to the question which of the two terms is more important, the reply is therefore that the relative importance of these terms depends strongly on the molecular system and on the temperature of deposition. Physically the dipole term

Table 2. Values of μ_0, the gas-phase dipole moment, α, the molecular polarisability, Ω, the molecular volume, s, the layer spacing between successive ML and μ, the dipole moment in the solid for various species as shown. $\langle E_{sym}\rangle$, $\langle E_{asym}\rangle$ or s (see text) and ζ are fitting parameters defined in Section 4. Uncertainties in values of $\langle E_{sym}\rangle$, $\langle E_{asym}\rangle$ and ζ parameters are mentioned in the text.

	N_2O	CF_3Cl	CF_2Cl_2	$CFCl_3$	Methyl formate: $HCOOCH_3$
μ_0	0.166 D	0.500 D	0.510 D	0.45 D	1.766 D
α	3.31 Å^3	4.740 Å^3	6.370 Å^3	7.913 Å^3	5.25 Å^3
Ω	37.79 Å^3	121.36 Å^3	130.78 Å^3	140.6 Å^3	103 Å^3
s	0.32 nm	0.31 nm	0.28 nm	0.25 nm	0.244 nm
μ	0.0785 D	0.181 D	0.119 D	0.025 D	0.354 D
$\langle E_{sym}\rangle$	5.43×10^8 V/m	-6.96×10^7 V/m	-7.00×10^7 V/m	-1.05×10^8 V/m	1.206×10^7 V/m
$\langle E_{asym}\rangle$	7.88×10^8 V/m	-5.63×10^8 V/m	-2.88×10^8 V/m	-1.73×10^8 V/m	1.148×10^9 V/m
ζ	43.8	500	900	1550	14,500

$\langle E_{sym}\rangle\zeta(\langle\mu_z\rangle/\mu)^2$ may be interpreted as a measure of the tendency of one dipole to restrict the angular motion of another, a 'locking' term or, as it is sometimes called, a 'frustration' term.

We now turn to the second term in the local field acting on a dipole, recollecting that this term is the measured field that arises through macroscopic spontaneous dipole alignment. This field resembles the Weiss field in ferromagnetism, which is assumed to be proportional to the magnetisation [67]. In this context, read degree of dipole alignment for magnetisation and read polarisation field for the Weiss field. We emphasise that the polarisation field, that is, the spontelectric field, is self-generated within the spontelectric material and takes the place of an external field imposed on the film [63]. The polarisation field is naturally opposed to the local symmetric field since the action of the spontaneous field created through macroscopic polarisation must, through Le Chatelier's principle, be to reduce the perturbation due to the electric field to a minimum and thus the electrical energy of the system, given by $\frac{1}{2}\varepsilon\varepsilon_0E_z^2$, to a minimum. Here E_z is the total local electric field in the z-direction, recollecting that E_x and E_y are taken to be zero by symmetry. All subsequent equations are written for simplicity in atomic units for which the Boltzmann constant is unity.

From the above, the net local field experienced by an average dipole is written as follows:

$$E_z = \langle E_{sym}\rangle\left[1+\zeta\left(\frac{\langle\mu_z\rangle}{\mu}\right)^2\right] - \langle E_{asym}\rangle\frac{\langle\mu_z\rangle}{\mu} \tag{1}$$

The second term is the backward–forward asymmetric field created by the average dipoles and experienced by the average dipole. Just as for $\langle E_{sym}\rangle$ and ζ, $\langle E_{asym}\rangle$ is a fitting parameter of the model designed to reproduce the value of $\langle\mu_z\rangle/\mu$, and hence the observed electric field in the film, the latter given by $\langle E_{asym}\rangle\langle\mu_z\rangle/\mu$.

Our stated aim is to reproduce the variation of the observed field with deposition temperature. For this purpose, the effect of thermal energy is now introduced. Thermal energy tends to limit the degree of dipole alignment where the value of dipole alignment is governed by the well-known Langevin equation derived, for example, in Ref. [63]. Thus,

$$\frac{\langle \mu_z \rangle}{\mu} = \coth\left(\frac{E_z \mu}{T}\right) - \left(\frac{E_z \mu}{T}\right)^{-1} \tag{2}$$

Note that $\langle \mu_z \rangle / \mu \to 0$ implies $E_z \to 0$ from Equation (2), which itself requires that $\langle E_{\text{sym}} \rangle \to 0$ from Equation (1). This represents the requirement in the mean field picture that the symmetric field, in the absence of dipole alignment, falls to zero when averaged over the film.

The ansatz is introduced that $\langle E_{\text{sym}} \rangle$, ζ and $\langle E_{\text{asym}} \rangle$ are temperature independent. Evidently the environment of the average dipole will change with temperature and therefore this ansatz can only be justified in terms of expediency. At any rate it may be tried out; it is found to work well for modelling N_2O data but less well, for example, for methyl formate, especially at higher temperatures, as we discuss in detail in Section 4.2.3.

It was mentioned earlier that μ is the dipole of the molecule in its environment in the amorphous solid as opposed to the gas phase. The relationship between the measured gas phase dipole moment and the generally unknown dipole moment of the molecule in a solid environment has been recently discussed in Ref. [68]. Essentially, as noted earlier, any particular dipolar species is surrounded by other dipolar species whose presence creates an electric field at the site of a chosen molecule. This molecule reacts so as to minimise the perturbation created through the local electric field. Thus the local electric field is opposed through a rearrangement of molecular charge whose effect is to depolarise the molecule, that is, to reduce its dipole moment. The difficulty is to estimate by how much the dipole is reduced from the gas-phase value. Evidently, this depends on E_z, the perturbing field given in Equation (1), itself coupled to the degree of dipole alignment via Equation (2). Indeed, it has been shown that the perturbation to the gas-phase value of the dipole moment, μ_0, is proportional through the molecular polarisability, α, to the perturbing field [20]. Our tactic is artificially to decouple the value of μ from the value of $\langle \mu_z \rangle / \mu$ and hold μ at a constant value irrespective of the changing temperature and associated environment, essentially an extension of the ansatz of the temperature independence of $\langle E_{\text{sym}} \rangle$, ζ and $\langle E_{\text{asym}} \rangle$. The relationship between μ_0 and μ used here is that proposed in Ref. [68]:

$$\mu = \frac{\mu_0}{1 + \alpha k / s^3} \tag{3}$$

where k was originally determined by Topping [69] and a value of $k = 11.034$ is used here. This value derives from an analysis that involves dipole–dipole interactions only and depends weakly on the assumed geometry of the array of molecular dipoles. s is a 'layer spacing' which can be roughly related to the molar volume. It is, however, left as a free parameter in the model since it can be analytically connected to $\langle E_{\text{asym}} \rangle$ as we show below. Equation (3) can imply a major difference between the gas-phase and solid-state dipole moment. For example, methyl formate has a gas phase dipole moment of 1.766 Debyes (5.891×10^{-30} Cm, 0.6949 au) and Equation (3) yields a dipole moment in solid methyl formate of 0.354 D, given $s = 0.244$ nm (derived from fitting, see below) using $\alpha = 5.25 \times 10^{-30}$ m^3.

A description is now given of how the electric field, E_{obs}, can be related to the degree of dipole alignment, $\langle \mu_z \rangle / \mu$. As noted in Section 2, the field is assumed to be given by the surface potential divided by the film thickness, itself equal to the number of ML times the layer spacing, s. The macroscopic polarisation, P_{obs}, is the effective charge per unit area which may be equated with the component $\langle \mu_z \rangle$ of the dipole moment divided by the volume of the

molecule, Ω. Moreover $P_{obs} = \varepsilon_0 E_{obs}$. Thus, $E_{obs} = \langle \mu_z \rangle / \Omega \varepsilon_0$ or $\langle \mu_z \rangle / \mu = \varepsilon_0 E_{obs} \Omega / \mu$, giving the desired relationship between degree of dipole alignment and the observed field. Since we use a depolarised value of μ, Equation (3), this simulates the response of the medium to an applied field and effectively introduces a local field correction. Thus a static permittivity does not figure in the above. One may note that the relationship between E_{obs} and $\langle \mu_z \rangle / \mu$ given is essentially a rewriting of the Helmholtz equation for the change in potential across a dipolar film [70,71].

Since the observed field is $\langle E_{asym} \rangle \langle \mu_z \rangle / \mu$ and $\langle \mu_z \rangle / \mu = \varepsilon_0 E_{obs} \Omega / \mu$, it follows that $\langle E_{asym} \rangle = \mu / \varepsilon_0 \Omega$. Now, μ depends on s, the layer spacing, via Equation (3) and therefore $\langle E_{asym} \rangle$ and s are not independent parameters, as noted earlier. Hence in fitting experimental data to the model there are in principle only three independent parameters, $\langle E_{sym} \rangle$, ζ and $\langle E_{asym} \rangle$ or s. Note that the electric field is referred to as the 'observed field', E_{obs}, but strictly contains the value of the fitting parameter s. We now proceed to examples of the variation of the degree of dipole alignment and the electric field in N_2O, the three chlorofluorocarbons (CFCs) CF_3Cl, CF_2Cl_2, $CFCl_3$ and methyl formate as a function of deposition temperature, in order to illustrate the use of the model described earlier. We leave the theoretical development necessary for an understanding of the switch of $d\langle \mu_z \rangle / \mu / dT$ from the expected negative value to the observed positive value for methyl formate to the section devoted to that species (Section 4.2.3).

The above model ignores the nature of the substrate on which N_2O or other material is laid down, by implication requiring that observed potentials are independent of the nature of the substrate. Also implicit in the model is the assumption that the effective dipole moment of N_2O (say) is the value engendered through the N_2O environment without any substrate influence. Thus, the model is only for bulk material and, within the confines of the model, the degree of dipole alignment should be independent of the nature of the substrate. This is corroborated by experiments involving Xe layers separating the gold substrate from N_2O as described in Section 3.1, with further evidence mentioned in Section 3.7 in which a heterostructure was introduced.

4.2. *Applications of the model*

4.2.1. *N_2O films*

Figures 21 and 22 show the result of a fit obtained using data between 38 K and 52 K for the electric field and degree of dipole alignment respectively. Data at 57, 60, 63 and 65 K have been excluded from the fit since, at these temperatures, which closely approach sublimation, fluctuations in local dipole orientation become large and mean field theory cannot be expected to hold. Indeed, experimental values of $\langle \mu_z \rangle / \mu$ drop increasingly rapidly above 60 K.

The parameters associated with the fits in Figures 21 and 22 are $\langle E_{sym} \rangle = 5.43 \pm 0.2 \times 10^8\ Vm^{-1}$, $\langle E_{asym} \rangle = 7.88 \pm 0.3 \times 10^8\ Vm^{-1}$ and $\zeta = 43.8 \pm 3.0$ as shown in Table 2, where the errors quoted are random errors and do not include systematic errors in the film thickness. At 40 K, the part of the field governed by $\langle E_{sym} \rangle$ and ζ is $1.27 \times 10^9\ Vm^{-1}$, which we refer to as the symmetric contribution, and the asymmetric term is $9.78 \times 10^7\ Vm^{-1}$ with reference to Equation (1) and the value of $\langle \mu_z \rangle / \mu$ of 0.1242 shown in Table 3. Thus, at 40 K,

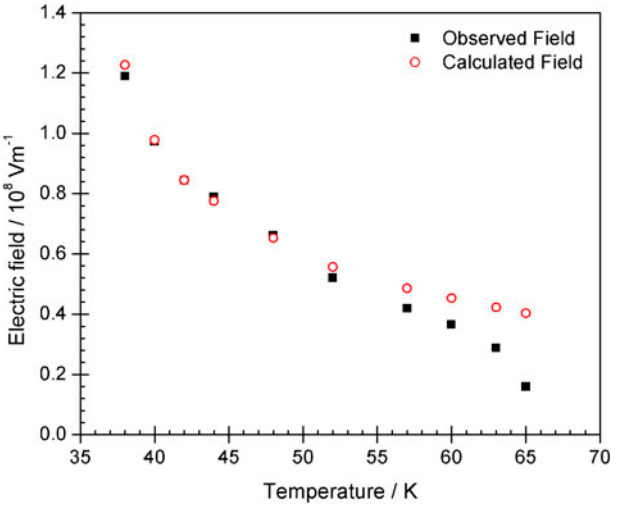

Figure 21. (Colour online) Electric fields in N_2O (black squares) and calculated values (red open circles) as a function of the temperature at which films of N_2O were laid down. Systematic errors due to uncertainties in film thickness may yield errors of up to 30% in absolute values of electric fields. Random errors in electric fields vary from 1% at low temperature to 5% at the highest temperatures.

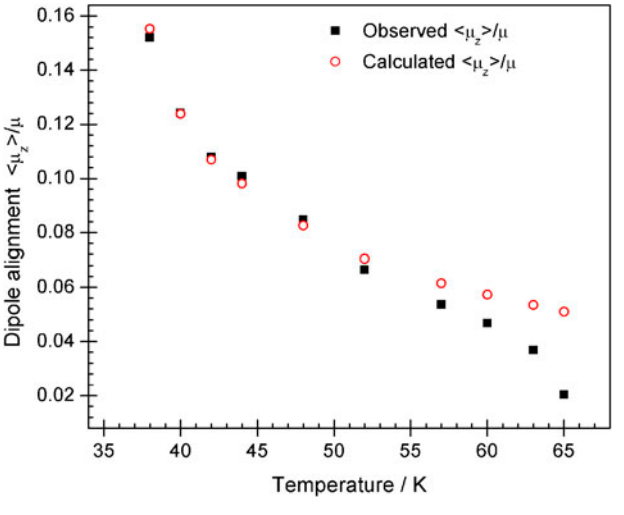

Figure 22. (Colour online) Degree of dipole alignment estimated from experiment in N_2O (black squares) and calculated values (red circles) as a function of the temperature at which films of N_2O were laid down.

the symmetric contribution to the local field is approximately an order of magnitude larger than the asymmetric contribution. This remains true throughout the temperature range over which the model is applicable, that is, up to 52 K.

Table 3. The variation of the electric field, E_{obs}, and degrees of dipole alignment, $\langle\mu_z\rangle/\mu$, as a function of deposition temperature for N_2O, compared with fits obtained using Equations (1) and (2) (Section 4.1) and values of parameters in Table 2. Data are shown graphically in Figures 21 and 22.

Temperature/K	Obs. field / Vm^{-1}	Calc. field / Vm^{-1}	$\langle\mu_z\rangle/\mu$ from observations	$\langle\mu_z\rangle/\mu$ calculated
38	1.189×10^8	1.227×10^8	0.1520	0.1552
40	9.723×10^7	9.783×10^7	0.1242	0.1238
42	8.436×10^7	8.448×10^7	0.1078	0.1069
44	7.889×10^7	7.754×10^7	0.1008	0.0981
48	6.616×10^7	6.529×10^7	0.0846	0.0826
52	5.205×10^7	5.567×10^7	0.0665	0.0704
57	4.196×10^7	4.859×10^7	0.0536	0.0615
60	3.655×10^7	4.530×10^7	0.0467	0.0573
63	2.882×10^7	4.228×10^7	0.0368	0.0535
65	1.598×10^7	4.034×10^7	0.0204	0.0510

Calculated values of $\langle\mu_z\rangle/\mu$ and electric field, $\langle E_{asym}\rangle\langle\mu_z\rangle/\mu$, are shown in Table 3. The experimental values of the spontelectric field, E_{obs}, are reproduced simultaneously with $\langle\mu_z\rangle/\mu$ to better than a few per cent for temperatures $\leqslant 52$ K.

4.2.2. *CFC films: CF_3Cl, CF_2Cl_2 and $CFCl_3$*

The study of the CFCs addresses the following fundamental question regarding spontelectrics: is the influence of the detailed chemical structure of the constituent species seminal to the nature of their spontelectric behaviour rather than purely their dipole moments? In this connection, CF_3Cl, CF_2Cl_2 and $CFCl_3$ have very similar gas-phase dipole moments of 0.500D, 0.510D and 0.45D, respectively. These species also possess similar electronic structure exemplified by the similarity of their absorption spectra [72].

Figures 23, 24 and Table 4 show the result of fits obtained using all data between 40 and 65 K for the three CFCs studied. The parameters associated with the fits in Figures 23 and 24 are given in Table 2. Random errors associated with values of parameters lie between 2% and 4%. It is evident from Figure 23 that the three CFCs possess spontelectric fields which lie in the order $CF_3Cl > CF_2Cl_2 > CFCl_3$, for example in the ratio ca. 9:4:1 at 45 K for CF_3Cl and CF_2Cl_2 and 46 K for $CFCl_3$. One important factor in this difference in spontelectric behaviour is the depolarisation of the molecules in the solid phase. Increased chlorination leads to an increased polarisability (Table 2) and therefore increased depolarisation in $CFCl_3$, yielding a smaller dipole moment in the solid. No such regularity is, however, apparent in the relative size of terms in E_z (Equation (1)). Thus the 'locking' field which hinders rotation, $\langle E_{sym}\rangle\zeta(\langle\mu_z\rangle/\mu)^2$, is -8.7×10^7 V/m, -1.33×10^8 V/m and -5.3×10^7 V/m for CF_3Cl, CF_2Cl_2 and $CFCl_3$, respectively, at 45 K (or 46 K for $CFCl_3$) using values in Tables 2 and 4. Evidently interplay between the symmetric and asymmetric terms leads to the observed behaviour through the feedback inherent in Equations (1) and (2). We conclude that the spontelectric characteristics of the three apparently closely related CFCs depend critically on intermolecular chemical forces that are not directly reflected in the similar gas-phase dipole moments of the individual molecules.

Table 4. The variation of the electric field, E_{obs}, and degrees of dipole alignment, $\langle\mu_z\rangle/\mu$, as a function of deposition temperature for the three CFCs, compared with fits obtained using Equations (1) and (2) (Section 4.1) and values of parameters in Table 2. Data are shown graphically in Figures 23 and 24

Temperature/K	Obs. field / Vm^{-1}	Calc. field / Vm^{-1}	$\langle\mu_z\rangle/\mu$ from observations	$\langle\mu_z\rangle/\mu$ calculated
CF_3Cl				
40	-4.25×10^7	-4.62×10^7	0.075	0.081
45	-3.28×10^7	-2.82×10^7	0.058	0.050
47.5	-1.97×10^7	-1.60×10^7	0.035	0.028
50	-7.55×10^6	-1.12×10^7	0.013	0.020
CF_2Cl_2				
45	-1.43×10^7	-1.46×10^7	0.042	0.046
55	-9.98×10^6	-8.19×10^6	0.029	0.024
60	-5.51×10^6	-5.33×10^6	0.016	0.016
65	-4.07×10^6	-4.55×10^6	0.012	0.013
$CFCl_3$				
43	-5.32×10^6	-5.29×10^6	0.031	0.031
46	-3.36×10^6	-3.18×10^6	0.019	0.018
50	-1.86×10^6	-2.19×10^6	0.011	0.013

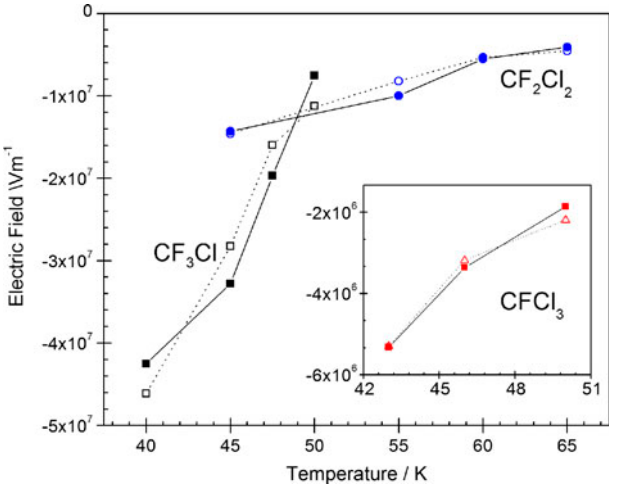

Figure 23. (Colour online) The variation of the electric field, E_{obs}, as a function of deposition temperature for CF_3Cl, CF_2Cl_2 and $CFCl_3$, using values in Table 2, compared with fits obtained using Equations (1) and (2). Fits are shown as open symbols and experimental values as solid symbols. Fitting parameters $\langle E_{sym}\rangle$, $\langle E_{asym}\rangle$ and ζ are given in Table 2.

The abrupt onset of temporal instability with deposition temperature of the spontelectric nature of $CFCl_3$ (Figure 15) arises from the fragility of the spontelectric system, attendant on a weak spontelectric field coupled with a weak solid state dipole. The temporal change from spontelectric structure to non-spontelectric, seen in Figure 15, comes about through a reloca-

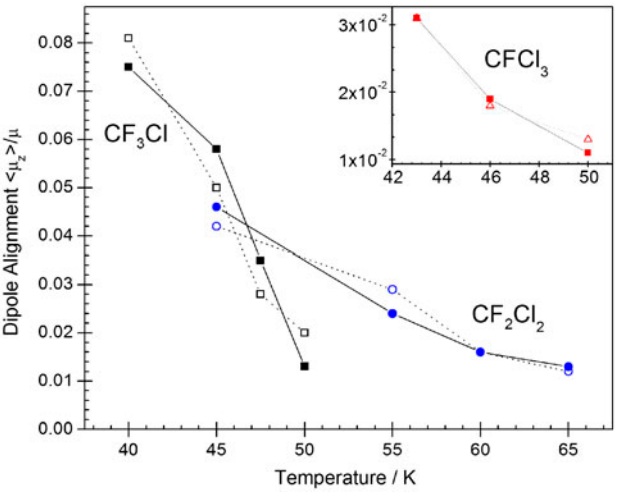

Figure 24. (Colour online) Degrees of dipole alignment estimated from experiment in the three CFCs (closed symbols) and calculated values (open symbols) as a function of the temperature at which films were laid down.

Table 5. Values of the symmetrical part, $\langle E_{\text{sym}}\rangle[1+\zeta(\langle\mu_z\rangle/\mu)^2]$ of the electric field E_z, Equation (1), and the asymmetrical part or the spontelectric field $\langle E_{\text{asym}}\rangle\langle\mu_z\rangle/\mu$ and the relative magnitudes of these terms for the three CFCs and for N_2O.

Temperature/K	Symmetrical term (V/m)	Asymmetrical term (spontelectric field) V/m	Ratio
CF_3Cl			
40	2.98×10^8	4.56×10^7	0.153
45	1.57×10^8	2.82×10^7	0.180
47.5	9.69×10^7	1.58×10^7	0.163
50	8.35×10^7	1.13×10^7	0.135
CF_2Cl_2			
45	2.03×10^8	1.32×10^7	0.065
55	1.06×10^8	6.91×10^6	0.065
60	8.61×10^7	4.61×0^6	0.054
65	8.06×10^7	3.74×10^6	0.046
$CFCl_3$			
43	2.61×10^8	5.36×10^6	0.021
46	1.58×10^8	3.11×10^6	0.019
50	1.33×10^8	2.25×10^6	0.017
N_2O			
38	1.09×10^9	1.19×10^8	0.109
40	9.10×10^8	9.72×10^7	0.107
42	8.19×10^8	8.44×10^7	0.103
44	7.85×10^8	7.89×10^7	0.101
48	7.13×10^8	6.62×10^7	0.093
52	6.48×10^8	5.21×10^7	0.080

tion of the dipoles to form a structure in which dipoles are no longer aligned. This may be a disordered structure or a crystalline state. The relative values of symmetric and asymmetric terms in E_z (Equation (1)) may be taken as a measure of this relocation to be a feasible event. Inserting values of $\langle E_{\mathrm{sym}}\rangle$, $\langle E_{\mathrm{asym}}\rangle$, ζ and $\langle \mu_z\rangle/\mu$ from Tables 2 and 4 gives values in Table 5 of the symmetric terms and asymmetric terms in E_z and their ratio for the three CFCs. Values for N_2O are also shown for comparison.

A clear decrease in an average value of 0.158 to 0.019 may be derived from data in Table 5 in the ratio of the symmetric to asymmetric contribution to E_z on moving from CF_3Cl to $CFCl_3$. Results in Table 5 suggest an onset of collapse of the spontelectric structure when the asymmetric term in Equation (1) becomes <1.9% of the symmetric. In summary, it is evident that for $CFCl_3$ a combination of sensitivity to motional fluctuations and the weakness of the asymmetric field, that is, the estimated spontelectric field, itself a reflection of the low values of $\langle \mu_z\rangle/\mu$, is the root cause of the different behaviour encountered in this species compared with CF_3Cl or CF_2Cl_2. Values for N_2O lie between those of CF_3Cl and CF_2Cl_2 and emphasise the variety of behaviour found in spontelectrics depending on chemical structure.

In order to model spontelectric effects, it would therefore appear essential to perform sophisticated calculations of solid-state structures including an accurate description of medium to long-range forces special to any system. For the present, experimental data remain the only means to establish the existence of a range of conditions for which spontelectric behaviour is found.

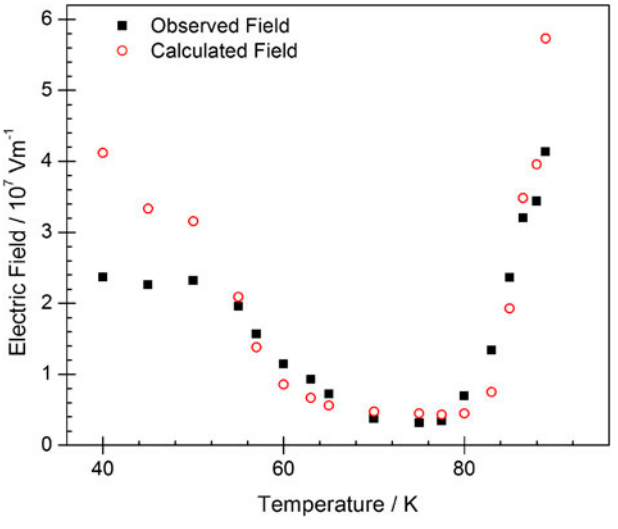

Figure 25. (Colour online) The variation of the observed electric field, E_{obs}, as a function of deposition temperature for methyl formate. Data are taken from Figures 10–12, with additional data not shown in those figures. Fits to experiment using the theory described in Section 4 are red open circles. Values of fitting parameters are given in Table 2. The lack of fit between theory and experiment at $\leqslant$50 K is discussed in Section 3.4; see also the Curie point data in Figure 20. An accurate fit between theory and experiment for $T > 80$ K may be obtained by relaxing the assumption that parameters of the model are temperature independent (Section 4.2.3).

4.2.3. *Applications to cis-methyl formate*

Methyl formate films show the unexpected property that the gradient with temperature of the spontelectric field and degree of dipole alignment switches from negative to positive at a critical deposition temperature [11] as seen in Figures 10–12. This critical temperature is around 78–80 K with an associated $\langle\mu_z\rangle/\mu \sim 0.003$. By contrast, the simple picture presented in the preceding sections would appear to require that increased thermal disorder would lead to weaker spontelectric behaviour; yet here the opposite behaviour with temperature of deposition is observed. This behaviour is illustrated in Figures 25 and 26 using results derived from the experimental data in Figures 10–12 plus data for additional temperatures of deposition, where initial slopes of surface potential vs. film thickness have been used as appropriate. We now explore further the nature of the switch from negative to positive gradient of the spontelectric field and degree of dipole alignment with temperature.

An obvious tactic to analyse the results shown in Figures 25 and 26 is to obtain the total differential $d\langle\mu_z\rangle/\mu/dT$. Inserting Equation (1) into Equation (2) we obtain an implicit equation of the form $\langle\mu_z\rangle/\mu = f(\langle\mu_z\rangle/\mu, T)$. Implicit differentiation may be carried out using standard forms but caution is necessary since these standard forms naturally require that $\langle\mu_z\rangle/\mu = f(\langle\mu_z\rangle/\mu, T)$ is satisfied exactly. From a practical standpoint, high accuracy in the implicit equation is necessary in order to give quantitative results for the differential. The fit shown in Figure 26 is found to be inadequate to yield quantitative agreement between experimental values of $d\langle\mu_z\rangle/\mu/dT$, obtained by interpolation from the data in Figure 26, and those computed from the analytic form of the differential. Computed values of the gradient obtained by inserting derived values of $\langle E_{\text{sym}}\rangle$, $\langle E_{\text{asym}}\rangle$ and ζ into the differential function shown below, Equation (4), lie generally within a factor of 4–5 of observed values, but can be an order of magnitude in error. The switch from negative to positive slope appears at 80–83 K, rather than at the observed value of 78–80 K.

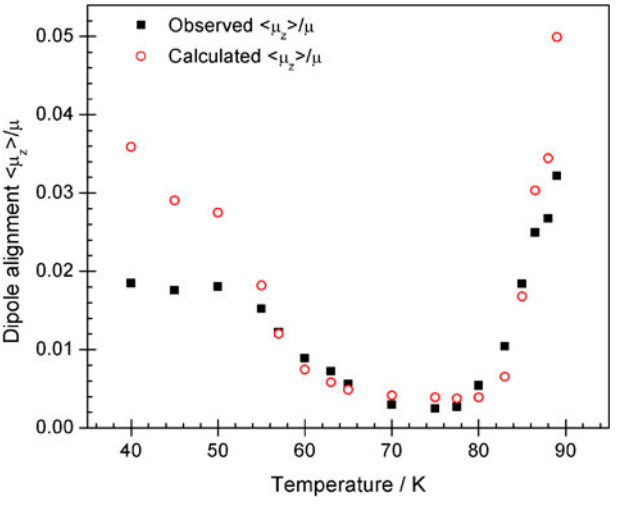

Figure 26. (Colour online) The variation of the degree of dipole alignment, $\langle\mu_z\rangle/\mu$, as a function of deposition temperature for methyl formate. Fits to experiment using the theory described in Section 4 are red circles. Values of fitting parameters are given in Table 2.

This quantitative breakdown may be ascribed to the ansatz that $\langle E_{\mathrm{sym}}\rangle$, $\langle E_{\mathrm{asym}}\rangle$ and ζ are temperature independent and by implication $\langle\mu_z\rangle/\mu$ independent. We return to this below where we show that relaxation of this assumption can result in accurate fitting. For the present, we proceed on the basis that the qualitative behaviour described by the analytical form of $d\langle\mu_z\rangle/\mu/dT$ remains descriptive of the physics. The total differential of $\langle\mu_z\rangle/\mu = f(\langle\mu_z\rangle/\mu, T)$ is given by

$$\frac{d\langle\mu_z/\mu\rangle}{dT} = \frac{1/\mu E_z - (\mu E_z/T^2)\mathrm{cosech}^2(\mu E_z/T)}{(\mu E'/T)\mathrm{cosech}^2(\mu E_z/T) - E'T/\mu E_z^2 - 1} \tag{4}$$

where $E' = \langle E_{\mathrm{asym}}\rangle - 2\zeta\langle E_{\mathrm{sym}}\rangle\langle\mu_z/\mu\rangle$ and E_z is defined by Equation (1). A significant property of Equation (4) is the presence of a singular cut in $\langle\mu_z\rangle/\mu$, T space for values which satisfy

$$(\mu E'/T)\mathrm{cosech}^2(\mu E_z/T) - E'T/\mu E_z^2 - 1 = 0 \tag{5}$$

A representation of $d\langle\mu_z\rangle/\mu/dT$ as a function of temperature and $\langle\mu_z\rangle/\mu$ is shown in Figure 27 using the fitted values of $\langle E_{\mathrm{sym}}\rangle$, $\langle E_{\mathrm{asym}}\rangle$ and ζ derived using Equations (1) and (2) and shown in Table 2. Figure 27 illustrates the set of singularities represented by Equation (5). Immediately to lower $\langle\mu_z\rangle/\mu$, T of this set, $d\langle\mu_z\rangle/\mu/dT$ is negative but is positive for higher $\langle\mu_z\rangle/\mu$, T on the other side of the singularity. Thus 'normal' and 'anomalous' behaviours are separated by the singular cut in Figure 27. Note that for the values of $\langle E_{\mathrm{sym}}\rangle$, $\langle E_{\mathrm{asym}}\rangle$ and ζ used here, the nominator in Equation (4) is positive for the entire range of $\langle\mu_z\rangle/\mu$ and T. Thus it is the sign change in the denominator which wholly governs the change of sign in $d\langle\mu_z\rangle/\mu/dT$.

Given that Equations (4) and (5) are of general (approximate) validity, it follows that any number of spontelectric materials may in principle share the common feature of a decreasing and then increasing degree of dipole alignment with increasing deposition temperature, separated by a singular cut. Thus, the anomalous behaviour reported for methyl formate is in principle a general characteristic of spontelectrics. We have not however –

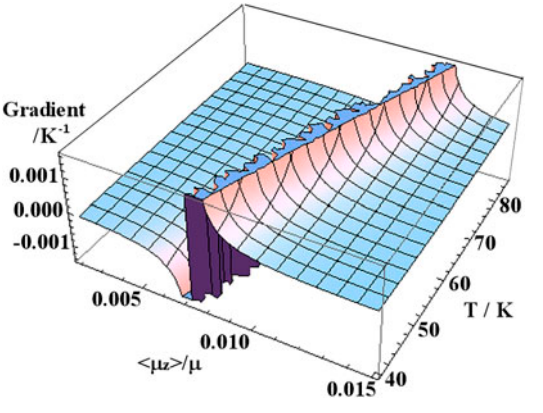

Figure 27. (Colour online) Methyl formate: the variation of the gradient $d\langle\mu_z\rangle/\mu/dT$, evaluated using Equation (4), as a function of the temperature, T, and the degree of dipole alignment $\langle\mu_z\rangle/\mu$, for values of $\langle E_{\mathrm{sym}}\rangle$, $\langle E_{\mathrm{asym}}\rangle$ (or equally, s, the layer spacing) given in Table 2.

so far – identified any other species that show this characteristic, noting that data in Figures 13 and 14 for ethyl formate and dihydrofuran are suggestive of the same behaviour, as noted in Section 3, but require detailed investigation to establish this. In connection with this, none of the three CFCs, whose spontelectric properties are discussed in the previous section, enters the regime in which the degree of dipole alignment increases with temperature of deposition. The regime of a positive value of $d\langle\mu_z\rangle/\mu/dT$ occurs at a critical degree of dipole alignment, given approximately by $\langle\mu_z\rangle/\mu = \langle E_{\text{asym}}\rangle/2\zeta\langle E_{\text{sym}}\rangle$ [11,12] that is, 0.008 for CF_3Cl, 0.0023 for CF_2Cl_2 and 0.0006 for $CFCl_3$. The lowest measured values of $\langle\mu_z\rangle/\mu$ are 0.02 for CF_3Cl at 50 K, 0.012 for CF_2Cl_2 at 65 K and 0.013 for $CFCl_3$ at 50 K. The inference is that, for these materials, collapse of the spontelectric structure intervenes, precluding achievement of the critical degree of dipole alignment associated with change in sign of $d\langle\mu_z\rangle/\mu/dT$.

An intriguing possibility arising from the behaviour shown in Figure 27 is that it may be feasible to cause the system abruptly to switch the gradient, $d\langle\mu_z\rangle/\mu/dT$, by provision of an external stimulus of an electric field. A trivial extension of the theory may be made by adding an arbitrary electric field, E_{ex}, to the expression for E_z in Equation (1), yielding a new Equation (4) in which in each case where E_z appears, $E_z + E_{\text{ex}}$ would now be found. Evidently, if a film of methyl formate is laid down which corresponds to a point in $\langle\mu_z\rangle/\mu$, T space close to the singular cut in Figure 27, application of an appropriate external field could cause the system to hover extremely close to the singularity or to flip from, say, a negative $d\langle\mu_z\rangle/\mu/dT$ to a positive $d\langle\mu_z\rangle/\mu/dT$. If we consider a deposition temperature of 85 K and use the observed gradient of $+4.5 \times 10^{-3}$ per K, then in order to induce a sign change in the gradient and create, for example, a value of -9×10^{-2} per K, an applied field, E_{ex}, of 760 V/mm, opposing E_z, would be required. This represents only a small perturbation to the system since the value of E_z in the unperturbed state is 50 times larger than this value of E_{ex}.

We now pose three questions designed to give insight into the change in sign of $d\langle\mu_z\rangle/\mu/dT$ at a critical temperature. The first question is this: what fundamental aspect of the current model gives rise to the observed switching behaviour of the degree of dipole alignment or electric field with temperature? The second poses the question of whether a simple linearisation of the coth function in Equation (2), or equivalently the cosech functions in Equation (4), preserves the switch from negative to positive slope. The third question, already mentioned previously, relates to the relaxation of the approximation that the parameters of the model are temperature independent.

The answer to the first question is that the feedback between the dipole orientation and the term $\langle E_{\text{sym}}\rangle\zeta(\langle\mu_z\rangle/\mu)^2$ in E_z, is the feature which gives rise to the switch of gradient. Unfortunately we are not able to prove this rigorously as the following considerations show. If we substitute Equation (1) into Equation (2) we obtain

$$\frac{\langle\mu_z\rangle}{\mu} = \coth\left(\frac{\left[\langle E_{\text{sym}}\rangle(1+\zeta(\langle\mu_z\rangle/\mu)^2) - \langle E_{\text{asym}}\rangle\langle\mu_z\rangle/\mu\right]\mu}{T}\right) - \left(\frac{\left[\langle E_{\text{sym}}\rangle(1+\zeta(\langle\mu_z\rangle/\mu)^2) - \langle E_{\text{asym}}\rangle\langle\mu_z\rangle/\mu\right]\mu}{T}\right)^{-1} \tag{6}$$

the full differential of which is given by Equation (4). We now show that a critical point of this function cannot exist. In doing so, we argue that we may ignore the recursive nature of Equation (6) since we are considering differential variations in seeking a critical point. The condition for the existence of a critical point for the function on the rhs of Equation (6) may be shown to be

$$\begin{aligned}&\mathrm{cosech}^2\{\mu\left[\langle E_{\mathrm{sym}}\rangle(1+\zeta(\langle\mu_z\rangle/\mu)^2)-\langle E_{\mathrm{asym}}\rangle\langle\mu_z\rangle/\mu\right]/T\}\\&\quad=T^2/\left[\mu(\langle E_{\mathrm{sym}}\rangle(1+\zeta(\langle\mu_z\rangle/\mu)^2)-\langle E_{\mathrm{asym}}\rangle\langle\mu_z\rangle/\mu)\right]^2\end{aligned}\tag{7}$$

Writing the rhs of Equation (7) as T^2/ϕ^2 where $\phi = \mu\ [\langle E_{\mathrm{sym}}\rangle\ (1+\zeta(\langle\mu_z\rangle/\mu)^2)-\langle E_{\mathrm{asym}}\rangle\langle\mu_z\rangle/\mu]$, we find that Equation (6) is not a possible condition. This arises since $\mathrm{cosech}^2(\phi/T)=-1/3+T^2/\phi^2+\phi^2/15T^2$ …. Thus we conclude that a critical point rigorously does not exist for this function. Inserting values for methyl formate, we find that $\mathrm{cosech}^2(\phi/T)$ is, however, approximately equal to T^2/ϕ^2 since the latter term in atomic units = 45.4 at $T=70$ K and the next largest term in the expansion is $-1/3$. Using the approximation that $\mathrm{cosech}^2(\phi/T)\sim T^2/\phi^2$, one then finds that the discriminant is analytically zero and therefore that no information may be gained with regard to the combination $\langle\mu_z\rangle/\mu$ and T which can give rise to a maximum, minimum or saddle point. These results also naturally apply for the case of $\zeta=0$.

An alternative approach has therefore been adopted which involves the numerical exploration of the behaviour of the model setting $\zeta=0$, that is, in the absence of feedback between the degree of dipole alignment and the term related to the symmetric field. Numerical experiments have been performed for those combinations of $\langle E_{\mathrm{sym}}\rangle$, $\langle E_{\mathrm{asym}}\rangle$ (or layer spacing s) which lead to a non-monotonic change of electric field or degree of dipole alignment with temperature of deposition. These experiments show that for any such combination of $\langle E_{\mathrm{sym}}\rangle$ and $\langle E_{\mathrm{asym}}\rangle$, the electric field or degree of dipole alignment *increase* with temperature, reach a maximum and then *decrease* beyond a critical temperature. This is the reverse of observation, and thus the condition $\zeta>0$ is a necessary one in order to reproduce the behaviour with deposition temperature seen in Figures 25 and 26. Indeed one finds a continuous change from the convex $\zeta=0$ behaviour of electric field and degree of dipole alignment with deposition temperature to the observed concave behaviour. The model increasingly reproduces the observations as ζ is allowed to rise towards the best fit value of 14,500 given in Table 2.

The second question regarding the behaviour of electric field with deposition temperature concerns the linearisation of Equations (1) and (2). Writing $\phi=\mu[\langle E_{\mathrm{sym}}\rangle(1+\zeta(\langle\mu_z\rangle/\mu)^2)-\langle E_{\mathrm{asym}}\rangle\ \langle\mu_z\rangle/\mu]$ as above, we expand the Langevin function, $\mathrm{L}(\phi)=\coth(\phi)-1/\phi$ to first order. Thus we set $\mathrm{L}(\phi)=1/3\ \phi$, the approximation used to yield the Debye equation for the variation of polarisation with temperature. This yields $\langle\mu_z\rangle/\mu=\phi/3T$ and

$$\begin{aligned}\frac{d\langle\mu_z\rangle/\mu}{dT}=&-\mu[\langle E_{\mathrm{sym}}\rangle(1+\zeta(\langle\mu_z\rangle/\mu)^2)\\&-\langle E_{\mathrm{asym}}\rangle\langle\mu_z\rangle/\mu]/\{T[\mu(2\zeta\langle E_{\mathrm{sym}}\rangle\langle\mu_z\rangle/\mu-\langle E_{\mathrm{asym}}\rangle)-3T]\}\end{aligned}\tag{8}$$

This preserves the behaviour seen in Figure 27 since $d\langle\mu_z\rangle/\mu/dT$ tends to $\pm\infty$ for values of $|T[\mu(2\ \zeta\langle E_{\mathrm{sym}}\rangle\langle\mu_z\rangle/\mu-\langle E_{\mathrm{asym}}\rangle)-3T]|$ tending to zero. Therefore, even at the simplest level

of approximation, a switch in sign of $d\langle\mu_z\rangle/\mu/dT$ is predicted. The critical value of temperature, T_{crit}, for which the slope, $d\langle\mu_z\rangle/\mu/dT$, is infinite, that is, the temperature at which the switch from negative to positive slope occurs, is given by $(\mu/3)(2\zeta\langle E_{sym}\rangle\langle\mu_z\rangle/\mu - \langle E_{asym}\rangle)$. Note that this expression may also be derived by expanding cosech^2 to first order in T in Equation (5) which defines the singular cut in $d\langle\mu_z\rangle/\mu/dT$.

We may assess the accuracy of this linearisation by asking the question: what is the value of the degree of dipole alignment which gives rise to a singularity in $d\langle\mu_z\rangle/\mu/dT$ at the observed temperature, T_{crit}, of (say) 78 K? If values of constants derived from fitting using Equations (1) and (2) (Table 2) are inserted into $T_{crit} = (\mu/3)(2\zeta\langle E_{sym}\rangle\langle\mu_z\rangle/\mu - \langle E_{asym}\rangle)$, then a critical value of the dipole alignment $(\langle\mu_z\rangle/\mu)_{crit} = 0.0115$. The experimental value of $(\langle\mu_z\rangle/\mu)_{crit}$ is 0.00266 and the computed value, using the derived constants in Table 2 and Equations (1) and (2), is 0.00368. Thus a clear discrepancy arises from linearisation of the system of equations. We conclude that expansion of the cosech function to a linear function of its argument preserves the observed switching behaviour of the gradient $d\langle\mu_z\rangle/\mu/dT$ but results in an inaccurate formulation. Note that if ζ is set to zero in the above, the result is recovered that no condition can be found under which there is a critical value of temperature for switching, in agreement with our above conclusion that non-zero ζ is essential to reproduce the observed switching.

The third question addresses the problem that the model is inaccurate to a troubling extent for methyl formate in reproducing the observed variation of the degree of dipole alignment and electric field with deposition temperature, especially at higher temperatures (Figures 25 and 26). Given that the film has some non-zero derivative of volume vs. deposition temperature, it is evident the layer spacing, s, and therefore $\langle E_{asym}\rangle$, are temperature dependent. It also follows that $\langle E_{sym}\rangle$ and ζ are temperature dependent. The effective dipole moment, μ, will also change with temperature via change in the layer spacing via Equation (3). These temperature dependencies are a reflection of the property that all parameters depend on the physical separation and relative orientation of molecules in the solid and that each temperature of deposition gives rise strictly to a new structure of the material.

Numerical experiments show that experiment and model predictions for deposition temperatures between 83 and 89 K can be brought into agreement by allowing $\langle E_{sym}\rangle$ or s (but not ζ) to vary smoothly with temperature of deposition. Thus $\langle E_{sym}\rangle$ may be allowed to vary smoothly between 1.698×10^7 V/m and 8.852×10^6 V/m between 83 and 89 K to give agreement between observation and model within ~0.5%, holding other parameters constant, noting that the temperature independent value of $\langle E_{sym}\rangle$ is 1.206×10^7 V/m (Table 2). Again, agreement (to within ~3%) may be achieved, holding other parameters constant, by varying s between 2.15×10^{-10} m and 2.62×10^{-10} m in the same temperature range, where the fixed value for the global fit is 2.44×10^{-10} m (Table 2). The introduction of temperature dependence of $\langle E_{sym}\rangle$, ζ and s has no influence on the denominator of Equation (4). In the most general case in which all quantities $\langle E_{sym}\rangle$, ζ and s (which includes μ) are treated as temperature dependent, only the nominator is modified. Thus a significant general result is that the switch from negative to positive $d\langle\mu_z\rangle/\mu/dT$ with increasing temperature is robust to an introduction of temperature dependence of the model parameters. Thus the singular cut in $\langle\mu_z\rangle/\mu$, T space remains determined by Equation (5), with whatever values of parameters appropriate.

Setting to one side the introduction of temperature dependence of $\langle E_{sym}\rangle$, ζ, s, $\langle E_{asym}\rangle$ and μ, it is possible to build a qualitative physical description of the behaviour of methyl for-

mate at high temperatures. The model parameters crudely define the potential energy landscape of the film. The semi-quantitative agreement between observation and model shown in Figures 25 and 26, with temperature-independent values of $\langle E_{sym}\rangle$, $\langle E_{asym}\rangle$ and ζ, implies that for methyl formate the potential energy landscape is fundamentally unchanged for deposition temperatures >50 K. Molecules can sample more of this landscape at higher temperatures. This concept, exemplified by enhanced mobility of species condensing from the gas phase at and within the surface layers, has recently been developed in relation to glass formation through gas phase deposition [73,74]. This leads to the following qualitative description of the events which may cause the increase of $\langle \mu_z\rangle/\mu$ with T for a set of critical combinations of T, $\langle \mu_z\rangle/\mu$. Species as they attach from the gas phase to the surface evidently find it favourable at all temperatures to form a dipole-oriented structure. The formation of an energetically favourable, that is, an oriented system, is enhanced by weakly hindered diffusion, implying greater mobility and associated molecular motion. According to results in Refs. [74,75], these are the conditions which are found as gas-phase species condense to form solid material to a depth of a few nanometers, that is, 10–20 ML. In addition, effects of greater mobility are likely to be enhanced very close to the surface. Greater thermal diffusion in higher temperature films implies that species are able to explore a greater volume of phase space, overcoming barriers of frustration imposed by $\langle E_{sym}\rangle$ and ζ between metastable states. This in turn may increase the degree of dipole alignment that can be achieved in the system, overturning the tendency to greater disorder associated with higher temperature. At all events, according to the model presented here, such increased alignment at higher temperatures appears to be an intrinsic property of spontelectrics.

More extensive sampling of the potential landscape will also modify feedback between bulk electric field and dipole orientation. This is itself modulated in a temperature-dependent manner through the values of the interrelated parameters $\langle E_{sym}\rangle$, ζ, s, $\langle E_{asym}\rangle$ and μ. The model described earlier above is naturally a 'first order' description, ignoring, for example, the phenomenon that different values of $\langle \mu_z\rangle/\mu$ represent different structures and imply different values of the symmetric part of the potential. Moreover, the temporal decay of structures formed at 80 K and above suggests that systems initially enter metastable states in the energy landscape that then slowly percolate through a multiple minimum landscape towards ever more stable configurations. This is analogous to the behaviour described in Ref. [74], in which a figure of merit is introduced to gauge the extent to which a glass formed from gas-phase deposition has relaxed towards the global minimum energy structure. In this connection, it is known that between 90 K and 100 K methyl formate undergoes a phase change. This has been attributed to crystallisation [75]. Molecular dynamics simulations would be valuable to test the validity of the above conjectures. Note also that the local heat of adsorption makes a contribution to the dynamics, a factor that would be included in any molecular dynamics model.

5. Concluding comments

In this review of the current status of spontelectrics, we have endeavoured to place these materials in an historical and current perspective with regard to spontaneously polarised solid films. The conclusion has been drawn that spontelectrics constitute a new form of the solid state.

They are distinct in particular from ferroelectric materials, while acknowledging that some indications of spontelectric behaviour may perhaps be found in early work of Kutzner [15].

A model has been set out based upon the proposal that the spontelectric effect arises essentially from dipole alignment dictated by dipolar interactions. This is a primitive mean field model in which temperature variation is described in terms of the standard thermodynamic description given by the Langevin expression [63], combined with three temperature-independent parameters used to describe the field at any representative dipole. The new ingredient of this model, by comparison with other Ising type models, is the introduction of explicit feedback between the degree of dipole alignment and the symmetrical part of the field experienced locally by any dipole, represented by the term $\langle E_{\mathrm{sym}}\rangle\zeta(\langle\mu_z\rangle/\mu)^2$ in Equation (1). This in turn highlights the intrinsic dependence of the spontelectric effect on dipole–dipole interactions, which are seen as central in their influence on the structure of spontelectric films. In particular, the variation of spontelectric field with temperature for methyl formate cannot be described in the absence of the $\langle E_{\mathrm{sym}}\rangle\zeta(\langle\mu_z\rangle/\mu)^2$ term to which reference has just been made. The model reproduces experimental data with an acceptable degree of fidelity for the five species, N_2O, CF_3Cl, CF_2Cl_2, $CFCl_3$ and methyl formate for which it has been tested, showing that dipole alignment due to dipole–dipole interactions is very likely to be the origin of the spontelectric effect. By contrast, dipole alignment in comparable organic ferroelectrics is very largely instigated by interactions other than dipole–dipole; rather, structures arise which fortuitously lead to aligned dipoles [30].

The model deals through use of the Langevin expression only with equilibrium configurations of the solid film characteristic of a particular temperature. The model is not designed to treat Curie effects, since these involve non-equilibrium structures, which under sufficient temperature and associated mechanical stress give way to systems containing randomly oriented dipoles. Equally the model cannot treat the temporal evolution of a spontelectric system as it breaks free from some local equilibrium. Both these features may be described by molecular dynamics simulations. These are yet to be performed. Indeed in order to understand spontelectric effects in depth, it would appear essential to perform sophisticated calculations of solid state structures including an accurate description of medium to long range forces special to any system. This has already been noted in connection with the three CFCs that behave differently from one another despite their chemical similarity [12]. For the present as mentioned earlier, experimental data remain the only means to establish the existence of a range of conditions for which spontelectric behaviour is found.

Insight into the nature of spontelectrics may be gained by making an analogy with a free running saturated non-linear system, for example a strongly saturated interstellar hydroxyl maser [76]. In such a non-local, non-linear system, knowledge of the starting conditions is lost over a short physical extent compared with the total length of the system, lying along the normal to the film surface in the case of spontelectrics. The system maintains a constant condition through almost its entire length and locks into a rigid configuration from which it may not be displaced without some major perturbation. This has been described in Section 3.4 and such displacement may take place for example through heating represented by Curie temperature measurements such as those in Figures 17–20. By analogy with a saturated maser, gain is represented in the present case through the creation of electric field through dipole alignment and stimulated events through the electric field itself creating dipole alignment. Loss is through thermal motion that opposes dipole alignment as described in Section 4. So long as gain overcomes loss, the molecules self-organise into a spontelectric dipole-aligned structure.

In doing so, they lose memory of the initial state from which order emerged save that the nature of the film–substrate interface may influence the sign of surface potential. In this connection, the film–vacuum interface, at which deposition takes place, may be of greater importance in determining the sign of the surface potential. This follows since we have observed that spontelectric behaviour is characteristic of the material of which the film is composed and the magnitude of the spontelectric field is essentially independent of the surface on which it is laid down. This consideration emphasises the non-local nature of the spontelectric effect through which every component molecule contributes to the structure with long range communication provided through the spontelectric field.

There remain numerous aspects of spontelectrics to explore. There are now extensive data on heterogeneous materials, a foretaste of which was given in Section 3.7. Suffice it to say here that one may to a large extent dial up any required electric field structure. These results are presently under preparation for publication [56]. In addition, preliminary experiments have been performed to explore the behaviour of dilute systems of N_2O in Xe, which may shed light on the essentially three-dimensional nature of the network of interacting dipoles in the film. Other areas in which results may soon be available will be in neutron and X-ray scattering and atomic force microscopy of spontelectric films. These studies should indicate the degree of order in spontelectric films and the nature of that order, differentiating between the space and time averages mentioned in Section 4.1.

It is of course tempting to make any number of predictions of the future technological importance of spontelectric materials, with regard to nano-xerography and solid-state nano-traps among other presently speculative applications. Rather than yield to this temptation, which has led in a number of other instances to promises that have fallen as flat as they were unproven, it is probably more pertinent to state that in order for spontelectrics to make a major contribution to technological advance, an important requirement would be to identify the spontelectric effect at room temperature. The second advance might perhaps be to implement switching of the spontelectric field or of the derivative of the field by applying an external coercive electric field. Piezo- and flexoelectric phenomena may also arise through analogy with ferroelectric materials. It is possible, for example, that the application of high pressure or a strain gradient may induce materials to exhibit spontelectric fields at higher temperatures than recorded here. For the present, the spontelectric phenomenon remains one whose appeal is rather as pure science: spontelectrics are a new form of the solid state and these do not come every day.

Acknowledgements

With reference to our own work reported here, we gratefully acknowledge the help of H.C. Fogedby and A. Svane (Aarhus University) in aiding us to formulate the theory presented in Section 4. We also gratefully acknowledge support of the staff of the Aarhus Synchrotron Radiation Laboratory (ISA) without whom this work would not have been possible, the Danish Research Council, the LASSIE FP7 ITN network, grant number 238258 a Marie Curie Intra-European Fellowship 009786 (RB) and the Lundbeck Foundation (RB).

References

[1] D. Field, G. Mrotzek, D.W. Knight, D.W. Knight, S.L. Lunt, and J.-P. Ziesel, J. Phys. B: At. Mol. Opt. Phys. **21**, 171 (1988).

[2] D. Field, G. Mrotzek, D.W. Knight, S.L. Lunt, J.-P. Ziesel, and J.B. Ozenne, Meas. Sci. Technol. **2**, 757 (1991).
[3] S.V. Hoffmann, S.L. Lunt, N.C. Jones, D. Field, and J.-P. Ziesel, Rev. Sci. Instrum. **73**, 4157 (2002).
[4] D. Field, N.C. Jones, S.L. Lunt, and J.-P. Ziesel, Phys. Rev. **A64**, 022708 (2001).
[5] J.P. Ziesel, N.C. Jones, D. Field, and L.B. Madsen, Phys. Rev. Lett. **90**, 083201 (2003).
[6] D. Field and L.B. Madsen, J. Chem. Phys. **118**, 1679 (2003).
[7] R. Balog, P. Cicman, D. Field, N.C. Jones, L. Feketeova, K. Hoydalsvik, T.A. Field, and J.-P. Ziesel, J. Phys. Chem. **115**, 6820 (2011).
[8] R. Balog, P. Cicman, N.C. Jones, and D. Field, Phys. Rev. Lett. **102**, 073003 (2009).
[9] O. Plekan, A. Cassidy, R. Balog, N.C. Jones, and D. Field, Phys. Chem. Chem. Phys. **13**, 21035 (2011).
[10] D. Field, O. Plekan, A. Cassidy, R. Balog, and N.C. Jones, Europhys. News **42**, 32 (2011).
[11] O. Plekan, A. Cassidy, R. Balog, N.C. Jones, and D. Field, Phys. Chem. Chem. Phys. **14**, 9972 (2012).
[12] A. Cassidy, O. Plekan, R. Balog, N.C. Jones, and D. Field, Phys. Chem. Chem. Phys. **15**, 108 (2013).
[13] F.D. Veredrame and E.R. Nixon, J. Chem. Phys. **44**, 43 (1966).
[14] C.P. Smyth and C.S. Hitchcock, J. Am. Chem. Soc. **1934**, 56 (1084).
[15] K. Kutzner, Thin Solid Films **14**, 49 (1972).
[16] X. Su, L. Lianos, Y.R. Shen, and G.A. Somorjai, Phys. Rev. Lett. **80**, 1533 (1998).
[17] L. Onsager, D.L. Staebler, and S. Mascarenhas, J. Chem. Phys. **68**, 3823 (1978).
[18] M.J. Iedema, M.J. Dresser, D.L. Doering, J.B. Rowland, W.P. Hess, A.A. Tsekouras, and J.P. Cowin, J. Phys. Chem. B **102**, 9203 (1998).
[19] V.F.Petrenko and R.W.Whitworth, *Physics of Ice* (Oxford University Press, Oxford, 2006).
[20] J.R. MacDonald and C.A. Barlow, J. Chem. Phys. **39**, 412 (1963).
[21] A. Gross, *Theoretical Surface Science: A Microscopic Perspective* (Springer-Verlag, Berlin, 2003).
[22] G. McElhinney and J. Pritchard, Surf. Sci. **60**, 397 (1976).
[23] A. Vilan, A. Shanzer, and D. Cahen, Nature (London) **404**, 166 (2000).
[24] K. Demirkan, A. Mathew, C. Weiland, Y. Yao, A.M. Rawlett, J.M. Tour, and R.L. Oplia, J. Chem. Phys. **128**, 074705 (2008).
[25] I.H. Campbell, S. Rubin, T.A. Zawodzinski, J.D. Kress, R.L. Martin, D.L. Smith, N.N. Barashkov, and J.P. Ferraris, Phys. Rev. B **54**, R14321 (1996).
[26] J.X. Tang, C.S. Lee, and S.T. Lee, J. Appl. Phys. **101**, 064504 (2007).
[27] M. Gratzel, Nature **414**, 338 (2001).
[28] H. Ishii, N. Hayaski, E. Ito, Y. Washizu, K. Sugi, Y. Kimura, M. Niwano, Y. Ouchi, and K. Seki, Phys. Status Solidi A **2004**, 201 (1075).
[29] H. Yamane, H. Fukugawa, S. Kera, K.K. Okudaira, and N. Ueno, J. Appl. Phys. **99**, 093705 (2006).
[30] S. Horiuchi and Y. Tokura, Nat. Mater. **7**, 357 (2008).
[31] E. Ito and M. Iwamoto, J. Appl. Phys. **81**, 1790 (1997).
[32] E. Ito, Y. Washizu, N. Hayashi, H. Ishii, N. Matsuie, K. Tsuboi, Y. Ouchi, Y. Harima, K. Yamashita, and K. Seki, J. Appl. Phys. **92**, 7306 (2002).
[33] K. Yoshizaki, T. Manaka, and M. Iwamoto, J. Appl. Phys. **97**, 023703 (2005).
[34] Y. Okayabshi, E. Ito, T. Isoshima, and M. Hara, Appl. Phys. Express **5**, 055601 (2012).
[35] Xu. Zai-Quan, Fu-Zhou Sun, Jian Li, Shuit-Tong Lee, Yan-Qing Li, and Jian-Xin Tang, J. Appl. Phys. **99**, 203301 (2011).
[36] J. Grimblot, P. Alnot, R.J. Behm, and C.R. Brundle, J. Electron. Spectrosc. Relat. Phenom. **52**, 175 (1990).
[37] M. Michaud, P. Cloutier, and L. Sanche, Phys. Rev. B **49**, 8360 (1994).

[38] M. Michaud, P. Cloutier, and L. Sanche, Phys. Rev. B **44**, 10485 (1991).
[39] W.C. Simpson, T.M. Orlando, L. Parenteau, K. Nagesha, and L. Sanche, J. Chem. Phys. **108**, 5027 (1998).
[40] M.C. Deschamps, M. Michaud, and L. Sanche, J. Chem. Phys. **121**, 4284 (2004).
[41] R. Resta and D. Vanderbilt, in *Physics of Ferroelectrics: A Modern Perspective*, edited by K.M. Rabe, C.H. Ahn and J.-M. Triscone (Springer, Berlin, Germany, 2007).
[42] H. Lu, C.-W. Bark, D. Esque de los Ojos, J. Alcala, C.B. Eom, G. Catalan, and A. Gruverman, Science **336**, 59 (2012).
[43] M.J. Polking, M.-G. Han, A. Yourdkhani, V. Petkov, C.F. Kisielowski, V.V. Volkov, Y. Zhu, G. Carunutu, A.P. Alivisatios, and R. Ramesh, Nat. Mater. **11**, 700 (2012).
[44] K. Kobayashi, S. Horiuchi, R. Kumai, K. Fumitaka, Y. Murakami, and Y. Tokura, Phys. Rev. Lett. **108**, 237601 (2012).
[45] J.C. Burfoot, *Ferroelectrics* (van Nostrand Co. Ltd., Lonon, 1967).)
[46] Y.B. Chen, M.B. Katz, X.Q. Pan, R.R. Das, D.M. Kim, S.H. Baek, and C.B. Eom, Appl. Phys. Lett. **90**, 072907 (2007).
[47] L.M.Blinov, V.M. Fridkin, V. M. S.P.Palto, A.V. Bune, P.A. Dowben and S. Ducharme, Open Access Research Paper in Physics and Astronomy DigitalCommons, University of Nebraska, Lincoln, 2000. <http://digitalcommons.unl.edu/physicsducharme/51>
[48] V.V. Shvartsman and A.L. Kholkin, J. Appl. Phys. **108**, 042007 (2010).
[49] Y. Akishige and Y. Kamishina, J. Phys. Soc. Jpn. **70**, 3124 (2001).
[50] M. Michaud, E.M. Hébert, P. Cloutier, and L. Sanche, J. Appl. Phys. **100**, 073705 (2006).
[51] K. Radler and J. Berkowitz, J. Chem. Phys. **70**, 221 (1979).
[52] B.E. Kohl and C. Panja, *Numerical Data and Functional Relationships in Science and Technology. Group III, Condensed Matter* (Landolt-Börnstein, Springer, Heidelberg, 2006).
[53] A. Stamatovic and G.J. Schultz, Rev. Sci. Instrum. **41**, 423 (1970).
[54] J. Matuska, D. Kubata, and S. Matejcik, Meas. Sci. Technol. **20**, 015901 (2009).
[55] R.M. Marsolais, M. Deschenes, and L. Sanche, Rev. Sci. Instrum. **60**, 2726 (1989).
[56] A. Cassidy, O. Plekan, J. Dunger, R. Balog, N.C. Jones, and D. Field, *to be submitted*.
[57] K.Zhang and P. Charbonneau, (2011). <http://www.arxiv.com/PS_cache/arxiv/pdf/1102/1102.1405v1.pdf>.
[58] M.E. Lines and A.M. Glass, *Principles and Applications of Ferroelectrics and Related Materials* (Oxford Classic Texts in the Physical Sciences, Oxford, 2001).
[59] Xu. Yuhuan, *J.D. Mackenzie*, J. Non-Cryst. Solids **246**, 136 (1999).
[60] M. Dehghani, M. Afshari, Z. Abusara, N. Moazzen-Ahmad, and A.R.W. McKellar, J. Chem. Phys. **126**, 164310 (2007).
[61] R. Dawes, X.-G. Wang, A.W. Jasper, and T. Carrington, J. Chem. Phys. **133**, 134304 (2010).
[62] M.E. Lines, Phys. Rev. B **15**, 388 (1977).
[63] C. Kittel, *Introduction to Solid State Physics*, 3rd ed. (John Wiley, New York, 1968).
[64] E. Cohen de Lara and J. Vincent-Geisse, J. Phys. Chem. **1976**, 80 (1922).
[65] B.L. Maschhoff and J.P. Cowin, J. Chem. Phys. **101**, 8138 (1994).
[66] D. Fernandez-Torre, O. Kupiainen, P. Pyykkö, and L. Halonen, Chem. Phys. Lett. **471**, 239 (2009).
[67] H. Kliem, M. Kuehn, and B. Martin, Ferroelectrics **400**, 41 (2010).
[68] A. Natan, L. Kronik, H. Haick, and R.T. Tung, Adv. Mater. **19**, 4103 (2007).
[69] J. Topping, Proc. R. Soc. London Ser. A **114**, 67 (1927).
[70] O. Gershewitz, M. Grinstein, C.N. Sukenik, K. Regev, J. Ghabboun, and D. Cahen, J. Phys. Chem. B **108**, 664 (2004).
[71] O.N. Oliveira, D.M. Taylor, T.J. Lewis, S. Salvagno, and C.J.M. Stirling, J. Chem. Soc. Faraday Trans. 1 **1989**, 85 (1009).

[72] See the Max Planck Institute Mainz-UV–VIS Atlas of Gaseous Molecules, edited by H.K.Rudek, G.K.Moortgat and MPI für Chemie, Atmospheric Chemistry Division, Mainz, Germany. <http://www.atmosphere.mpg.de/enid/2295>).
[73] S.F. Swallen, K.L. Kearns, M.K. Mapes, Y.S. Kim, R.J. McMahon, M.D. Ediger, T. Wu, L. Yu, and S. Satija, Science **315**, 353 (2007).
[74] S. Singh and J.J. de Pablo, J. Chem. Phys. **134**, 194903 (2011).
[75] P. Modica and M.E. Palumbo, Astron. Astrophys. **519**, A22 (2010).
[76] D. Field and M.D. Gray, Mon. Not. R. Astron. Soc. **234**, 353 (1988).